Thermodynamics of a one-dimensional self-gravitating gas with periodic boundary conditions

Pankaj Kumar and Bruce N. Miller*

Department of Physics and Astronomy,

Texas Christian University, Fort Worth, Texas 76129, USA

Dan Pirjol

Department of Particle Physics, National Institute of Physics and Nuclear Technology, Bucharest, Romania

(Dated: July 29, 2016)

arXiv:1607.08490v1 [cond-mat.stat-mech] 29 Jun 2016

Abstract

We study the thermodynamical properties of a one-dimensional gas with one-dimensional gravitational interactions, and placed in a uniform mass background. Periodic boundary conditions are implemented as a modification of the potential consisting of a sum over mirror images (Ewald sum), regularized with an exponential cut-off. The system has a phase transition at a critical temperature. Above the critical temperature the gas density is uniform, while below the critical point the system becomes inhomogeneous. Numerical simulations of the model confirms the existence of the phase transition, and are in good agreement with the theoretical results.

PACS numbers: 05.70.Fh, 04.40.-b, 05.10.-a, 05.45.Pq

Keywords: Statistical mechanics; phase transition; N-body simulation; Lyapunov exponent

* b.miller@tcu.edu

I. INTRODUCTION

The thermodynamics of self-gravitating systems has been studied for a long time, starting with the classical analysis of Chandrasekhar [1]. An overview of the stability problem for such systems in three dimensions is given by Chavanis in [2]. The stability properties are found to be different in the canonical and microcanonical ensembles. In the canonical ensemble a self-gravitating system enclosed in a volume of radius R is unstable under collapse at energies below a critical value $E_c = -0.335GM^2/R$, the so-called Antonov instability.

The problem is simplified by working in a one-dimensional setting. The equilibrium thermodynamics of the one-dimensional gravitational gas has been studied for a bewildering variety of scalings and assumptions. We start by giving a brief summary of the results in the literature. For simplicity we restrict this summary to studies of the one-dimensional gravitational gas in thermal equilibrium. We also mention only studies where the equation of state of the gas is derived from first principles, as opposed to being one of the inputs of the analysis.

Salzberg [3] considered a one-dimensional gravitational gas of N particles of mass m enclosed in a finite volume L, and interacting by potentials $gm^2|x_i - x_j|$ with a hard core d. (Note that one-dimensional particles correspond to three-dimensional mass sheets which can move freely and cross each other). This leads to non-extensive thermodynamics in the limit $N \to \infty$ at fixed m. For example the total interaction energy scales like $U \simeq N^3$ as $N \to \infty$. The equation of state has the form $L = Nd + 2kT/p$, which is essentially the free gas equation of state corrected by the hard core volume $p = kT/(L - Nd)$. This is clearly not very realistic, so alternative scalings for the interaction gm^2 with N have been explored in the literature.

A different setting was adopted by Rybicki [4], who considered N particles of mass m moving along the infinite line and interacting by potentials $V(x, y) = gm^2|x - y|$ (no hard core). The $N \to \infty$ limit was taken at fixed total mass $M = Nm$ and total energy E (Vlasov limit). This corresponds to scaling the particle masses as $m = M/N$. The one-particle distribution function was computed, from which the density of the gas in thermodynamical equilibrium was obtained. Under the infinite volume setup assumed in [4], the equation of state of the gravitational gas was not considered in this paper.

Considering a gas enclosed into a finite volume $[0, L]$, the usual thermodynamical limit is $N, L \to \infty$ at fixed particle number density $\rho = N/L$. This limit was considered by Isihara [5] who studied the equilibrium thermodynamics of a one-dimensional gas enclosed in the box $[0, L]$ interacting with two-body potentials

$$V(x,y) = \begin{cases} -\frac{\mu}{L}\left(1 - \frac{1}{L}|x-y|\right) & , |x-y| > \delta \\ +\infty & , |x-y| < \delta \end{cases} \tag{1}$$

Apart from the constant term, this interaction is identical to the one-dimensional gravitational interaction with strength $2\pi G m^2$, under the scaling $m \sim 1/L$ for the particle masses which corresponds to fixed total particle mass $M = mN = m\rho L$. The advantage of this scaling is that it gives usual extensive properties for the gas energy and entropy.

The paper [5] derived the thermodynamical quantities of the gas with interaction (1) under certain special periodic boundary conditions, and concluded that the equation of state is van der Waals. The system has a liquid-gas phase transition. This is somewhat surprising, considering that no such phase transition is obtained for the one-dimensional gravitational gas in [4]. However, these systems differ in one important respect, as the interaction (1) has a hard core. In a wide class of interacting systems (systems of particles interacting by Kac potentials), a hard core is required in order to have a phase transition [6].

In order to study further this issue, a lattice gas version of the system considered in [5] was studied in [7]. This can be shown to be equivalent to a continuous one-dimensional gas enclosed in the box $[0, 1]$ with the interaction

$$V(x,y) = |x-y| - \xi \tag{2}$$

and with a special form of the entropy function, specific to the lattice gas. The constant ξ is an universal attractive interaction, which is felt by all particle pairs. Taking $\xi = 1$ reproduces the Isihara interaction (1), and taking $\xi = 0$ reproduces the interaction potential of the one-dimensional gravitational gas. The main result of [7] is that the system has a phase transition only for $\xi > 0$, while for $\xi = 0$ no such phenomenon is observed. The exact equation of state is obtained in the thermodynamical limit, which turns out to be different from a van der Waals equation, although it is qualitatively similar, and it approaches van der Waals form in the large temperature limit.

A scaling similar to that described above was proposed by de Vega and Sanchéz [8] in the context of *three-dimensional* systems by taking the thermodynamical limit $N, R \to \infty$ at fixed N/R, with R the size of the system. This is similar to the one-dimensional scaling considered above.

The equilibrium thermodynamics of the one-dimensional gravitational gas was also studied by Monahan [9], and by Fukui, Morita [10]. The paper [9] derived an exact lower bound on the partition function of the one-dimensional gravitational gas following from the Jensen inequality. As shown in [7], such a bound gives an accurate approximation which approaches the exact result in the large temperature limit.

Periodic boundary conditions are often used in practice to simplify the solution of statistical mechanics problems. With short-range interactions they can be shown to preserve the thermodynamical properties of the system, up to a surface term which has a subleading contribution in the thermodynamical limit [11]. While the gravitational interaction is long-ranged and does not satisfy the conditions under which the results of [11] are obtained, modifications of the one-dimensional interaction with periodic boundary conditions have been considered as well.

One of the best known models of this type in the literature is perhaps the HMF model with Hamiltonian [12]

$$H_{\rm HMF} = \sum_{i=1}^{N} \frac{1}{2} m v_i^2 + \frac{\gamma}{2N} \sum_{i<j} [1 - \cos(\theta_i - \theta_j)], \tag{3}$$

where $\theta_i \in (0, 2\pi)$. This corresponds to particles moving on a circle of unit radius and interacting by attractive potentials $V_{ij} = \frac{\gamma}{4N} d_{ij}^2$ where the distance between the particles is $d_{ij} = 2\sin(\frac{1}{2}(\theta_i - \theta_j))$. Note that the potential is quadratic in the distance, as opposed to linear as appropriate for one-dimensional gravity. A similar model is the self-gravitating ring model, where the particles are constrained to move on a circle, and interact by three-dimensional gravitational potentials [13].

We consider in this paper an alternative way of introducing periodic boundary conditions in the one-dimensional gravitational system, which was proposed by Miller and Rouet in [14], and has the advantage of preserving the linear dependence of the potential on the distance $d = |x-y|$ between particles for sufficiently small d. This corresponds to the following set-up: the system is enclosed in the box $[0, L]$ and has periodic boundary conditions. In addition, the system is assumed to be placed into the uniform background of a mass distribution.

The model is appropriate for studying one-dimensional density fluctuations in a uniform mass distribution and a Coulombic version of the model has been used to investigate single-component plasmas [15].

The Miller-Rouet model is somewhat similar to the OSC model (one dimensional static cosmology) which was introduced by Aurell et al [16–18] and studied further by Valageas in [19, 20]. This model differs from the former in how the periodic boundary conditions are implemented. Specifically, the periodicity is imposed by adding an external potential. In contrast, the Miller-Rouet model considered in this paper maintains the translation invariance and implements the periodic condition by modifying only the two-body interaction potential.

We use classical statistical methods to derive the thermodynamical properties of the system in the canonical ensemble. We determine the single particle distribution function by minimizing the free energy, and obtain explicit results for the free energy density and the equation of state of the gas. The system is homogeneous for temperatures larger than a critical temperature, and develops a position-dependent density below this temperature. The states with inhomogeneous density are states of thermodynamical equilibrium.

MD simulations are generally employed in the study of the systems that exhibit considerable chaotic dynamics needed to attain a phase-space equilibrium. A smaller finite-sized version of an otherwise ergodic-like system may have a segmented phase space with KAM tori separating the stable and unstable regions. For example, in a three-body version of the Miller-Rouet gravitational gas, it was shown that the phase-space always exhibits chaotic as well as stable regions and a KAM breakdown to complete chaos is not observed at any energy [21]. However, as the number of particles (N) is increased, the contribution from chaotic orbits increases drastically and any randomly selected initial condition results in a chaotic orbit with LCEs converging to a single universal value for a given energy [22]. Such behavior has also been shown for the free-boundary version of the one-dimensional gravitational gas system in which the phase space was found to be practically fully chaotic for $N \geq 5$ [23]. In general, caution must be taken while applying theoretical and MD methods to systems with segmented phase space.

Phase-space mixing leading to a relaxed state is a prerequisite for equilibrium statistical mechanics to apply to a system. Mixing in phase space arises as a result of dynamical instability in the phase space and is usually characterized by existence of at least one positive

Lyapunov characteristic exponent (LCE) [24]. For a Hamiltonian system with n degrees of freedom, a full Lyapunov spectrum may have up to $n-1$ positive LCEs [25, 26]. Of particular interest is the maximal positive LCE λ_1 which quantifies the largest average rate of exponential divergence of a given phase-space orbit with respect to the nearby orbits [23, 25, 27, 28].

Apart from being important from a dynamical perspective, LCEs also play an important role in thermodynamic studies and have been shown to serve as indicators of phase transitions [29–33]. For example, the largest LCE was shown to attain a maximum at the fluid-solid phase transition for a two-dimensional particle system [32]. The largest LCE has also been observed to display a transition-like variation at the critical temperature for a one-dimensional chain of coupled nonlinear oscillators [33]. In N-body simulations with a finite number of particles, LCEs have also been shown to exhibit behaviors that are observed in the thermodynamic limit [34, 35].

An exact numerical method of calculating the full Lyapunov spectrum was proposed for the case of one-dimensional gravitation gas [23] and the approach was further extended to the periodic-boundary versions of Coulombic and gravitational versions [22]. As we shall see in Sec. V D of this paper, we use the formulations presented in Ref. [22] to calculate the largest LCE and examine its temperature dependence for an indication of a phase transition.

The paper is structured as follows. For ease of reference we give an overview of the Miller-Rouet model and of its derivation in Section II. In Secs. III and IV, we formulate the statistical mechanics for the model in the canonical ensemble and derive its thermodynamical properties. We work in the Vlasov limit, by taking the particle number very large $N \to \infty$ at fixed total particles mass $M = Nm$. This leads to finite results for the energy and free energy per particle. The single particle distribution function, giving the gas density, is obtained by solving a variational problem for the free energy. In Sec. V, we verify the validity of the theoretical predictions by numerically computing the time-averaged values of such thermodynamic parameters as temperature, radial distribution function, and pressure in N-body simulations of the model using a molecular-dynamics (MD) approach. A few technical derivations are given in two Appendices.

II. THE MILLER-ROUET MODEL

We consider in this paper a one-dimensional gas of particles of mass m enclosed in a box $[0, L]$, and interacting with potential energy [14]

$$V(x,y) = 2\pi G m^2 \left(|y-x| - \frac{1}{L}(y-x)^2 - \frac{1}{6}L \right) . \tag{4}$$

This is the potential energy of a mass at position x due to the interaction with another particle at y and all its mirror images separated by the periodicity length L. The plot of the potential $V(x,y)$ is shown in Figure 1. At small distances $|x-y| \ll L$ it grows approximatively linearly, just as the one-dimensional gravitational potential, but for $|x-y| > L/2$ it becomes repulsive.

We recall briefly the derivation of this potential and its relation to one-dimensional gravitation. The potential $V(x,y)$ is the difference of two terms: the sum of the contributions from mirror images $V_0(x,y)$, and the contribution of the uniform background of mass $\Phi(x)$

$$V(x,y) = V_0(x,y) - 2\pi G m^2 \frac{1}{L} \int_{-\infty}^{\infty} dy |x-y| e^{-\kappa|x-y|} . \tag{5}$$

The interaction $V_0(x,y)$ gives the potential felt by a particle placed at y from a particle at x plus the infinite number of its mirror images, separated by L in both directions

$$V_0(x,y) = \sum_{k=-\infty}^{\infty} 2\pi G m^2 |x-y+kL| e^{-\kappa|x-y+kL|} . \tag{6}$$

The damping factor $e^{-\kappa|x-y+kL|}$ with $\kappa \to 0$ is introduced following [36] and has the advantage that it makes the sum over mirror images convergent.

The sum over mirror images can be evaluated in closed form with the result

$$\begin{aligned} &\sum_{k=-\infty}^{\infty} |x-y+kL| e^{-\kappa|x-y+kL|} \\ &= |x-y| e^{-\kappa|x-y|} + 2L \frac{e^{\kappa L}}{(e^{\kappa L}-1)^2} \cosh[\kappa(y-x)] - 2\frac{1}{e^{\kappa L}-1}(y-x)\sinh[\kappa(y-x)] \end{aligned} \tag{7}$$

where the first term is the contribution from the $n = 0$ term in the sum, and the remaining terms are the contributions from the mirror images of the particle at x. The proof of this result is given in the Appendix A.

Expanding (7) in the limit $\kappa \to 0$ and keeping only the terms which do not vanish in this limit we get

$$\lim_{\kappa \to 0} V_0(x,y) = 2\pi G m^2 \left(|y-x| - \frac{1}{L}(y-x)^2 + \frac{2}{\kappa^2 L} - \frac{1}{6}L \right) . \tag{8}$$

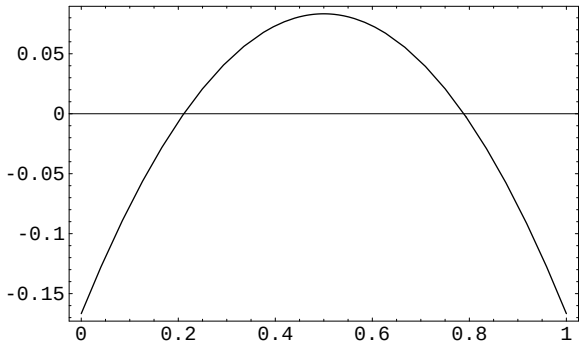

FIG. 1. Plot of the interaction energy $LV(x,y)$ vs $\frac{1}{L}|x-y|$ in the Miller, Rouet model.

The first term is the original linear attractive interaction, and the second term is a quadratic repulsive interaction, which vanishes in the limit of a very large periodicity radius $L \to \infty$. The physical meaning of this repulsive term is as follows. As two particles are separated by more than $L/2$, the attractive effect of their mirror images in the nearby cells overcomes the attractive interaction between them. This appears as a repulsive force when the distance satisfies $|x-y| > L/2$.

Finally we subtract the contribution of a uniform background of mass. This amounts to a interaction energy $\Phi(x)$ given by

$$\Phi(x) = \frac{2\pi G m^2}{L} \int_{-\infty}^{\infty} dy |y-x| e^{-\kappa|x-y|} = \frac{4\pi G m^2}{\kappa^2 L} \,. \tag{9}$$

This is a uniform potential, independent of position. The effect of subtracting the uniform background contribution $\Phi(x)$ from (8) amounts to canceling out the (positive) constant term $4\pi G m^2/(\kappa^2 L)$. The remaining constant term $-\frac{1}{6} 2\pi G m^2 L$ is negative and finite.

III. THERMODYNAMICS IN THE STATIC VLASOV LIMIT

We would like to derive the thermodynamical properties of a continuous gas enclosed in the $[0, L]$ volume, with periodic boundary condition, and interacting by the potential (4).

We work at fixed L and total particle mass $M = mN$. This implies that the particle masses scale as $m \sim 1/N$. Since both the inertial and gravitational mass are scaled, the dynamics of the system is the same as if the inertial mass is 1, and the particles interact by the potential

$$V(x,y) = 2\pi G M \frac{1}{N} \left(|x-y| - \frac{1}{L}(x-y)^2 - \frac{1}{6} L \right) . \tag{10}$$

This requires also that the temperature is rescaled as $T/m \to T$. In order to make this rescaling explicit, we will denote in this section the rescaled temperature as $T_V = T/m$ (the subscript stands for Vlasov temperature).

It is well known that a system with interaction of the form (10) can be described by a mean-field theory [37, 38]. The interaction potential scales like $\sim 1/N$ with the number of particles, at fixed volume L. In the limit $N \to \infty$ the energy per particle approaches a finite value, and the system is described by the one-particle distribution function $\rho(x)$, giving the probability of finding a particle in the volume element $[x, x + dx]$. This limiting procedure corresponds to the mean-field, or static Vlasov limit.

Assume that the system is at a given temperature T_V. The free energy per particle is

$$f = \frac{F}{N} = u - T_V s \tag{11}$$

where $f = f_{\rm Q} + f_{\rm kin}$ consists of a configurational contribution $f_{\rm Q}$ and a contribution from the kinetic degrees of freedom $f_{\rm kin} = k_B T_V(\log N - 1 + \frac{1}{2}\log(\frac{h^2}{2\pi k_B T_V}))$. The configurational contribution is given by the solution of the variational problem

$$f_{\rm Q} = \inf_\rho \left\{ \frac{1}{2}(2\pi GM) \int_0^L dxdy\rho(x)\rho(y) \left(|x-y| - \frac{1}{L}(x-y)^2 - \frac{1}{6}L \right) \right. \tag{12}$$
$$\left. + k_B T_V \int_0^L dx \rho(x) \log \rho(x) \right\}$$

where the infimum is taken over all functions $\rho(x)$ normalized as

$$\int_0^L dx \rho(x) = 1\,. \tag{13}$$

The solution of the variational problem (12) gives the single particle distribution function $\rho(x)$. This gives the so-called isothermal Lane-Emden equation for $\rho(x)$ [37, 38].

The energy $u = \frac{U}{N}$ and entropy $s = \frac{S}{N}$ per particle are easily obtained from the free energy f as $u = f - T_V \partial_{T_V} f$ and $s = -\partial_{T_V} f$. They are given by

$$u = \frac{1}{2}k_B T_V + \frac{1}{2}(2\pi GM) \int_0^L dxdy\rho(x)\rho(y) \left(|x-y| - \frac{1}{L}(x-y)^2 - \frac{1}{6}L \right) \tag{14}$$

$$s = -k_B \int_0^L dx \rho(x) \log \rho(x) + s_{\rm kin} \tag{15}$$

where $\rho(x)$ is the minimizer of the functional (12). The total energy per particle is the sum of the contribution from the kinetic energy, and the interaction energy with the remaining $N-1$ particles. The contribution of the kinetic degrees of freedom to the entropy per particle is $s_{\rm kin} = -\partial_{T_V} f_{\rm kin} = -k_B(\log N - \frac{3}{2} + \frac{1}{2}\log \frac{h^2}{2\pi k_B T_V})$.

A. Large temperature approximation

For temperatures $k_B T_V \gg 2\pi G M \frac{1}{4} L$ much larger than the range of variation of the potential $V(x,y)$, the density of the gas approaches a constant value $\rho(x) = 1/L$. Expressed in terms of the actual temperature $T = m T_V$ this condition reads $k_B T \gg \frac{1}{4} 2\pi G \frac{M^2}{N}$.

In this regime the thermodynamical properties of the gas simplify very much. The energy and entropy per particle become

$$u = \frac{1}{2} k_B T_V + \frac{1}{2} g^2 \int_0^L dx dy (|x-y| - (x-y)^2 - \frac{1}{6}) = \frac{1}{2} k_B T_V \tag{16}$$

$$s = k_B \log(L/N) + k_B \left(\frac{3}{2} - \frac{1}{2} \log \frac{h^2}{2\pi k_B T_V} \right) . \tag{17}$$

Note that the constant term $-\frac{1}{6}$ in the interaction energy cancels the contributions from the linear and quadratic terms, and the total interaction energy of the gas vanishes in the uniform density limit. The only contribution in (16) comes from the kinetic degrees of freedom.

The total free energy of the gas is

$$\begin{aligned} F = N(u - T_V s) &= \frac{1}{2} N k_B T_V - N k_B T_V \log(L/N) - N k_B T_V \left(\frac{3}{2} - \frac{1}{2} \log \frac{h^2}{2\pi k_B T} \right) \\ &= L \left(\frac{1}{2} k_B \bar{\rho} T_V + k_B T_V \bar{\rho} \log \bar{\rho} + k_B T_V \bar{\rho} \log \bar{\rho} \right) - L \bar{\rho} k_B T_V \left(\frac{3}{2} - \frac{1}{2} \log \frac{h^2}{2\pi k_B T_V} \right) . \end{aligned} \tag{18}$$

In the last line we introduced $\bar{\rho} = N/L$ the particle number density of the gas.

The pressure of the gas is

$$p(\bar{\rho}, T_V) = -(\partial_L F)_{N, T_V} = k_B \bar{\rho} T_V \, , \tag{19}$$

which is the ideal gas equation of state.

B. An energy-entropy argument

For temperatures T_V comparable to $2\pi G M \frac{1}{4} L$ and below, the thermodynamics of the system with interaction (4) is expected to be more complex. We give next a qualitative discussion based on an energy-entropy minimization argument. The equilibrium state is given in general by the minimum of the free energy $F = U - TS$. For $T = 0$ this corresponds to the minimum of U, while for $T \to \infty$ it corresponds to a maximum of the entropy S.

For small temperatures $T \to 0$ the equilibrium state of the system corresponds to a minimum of the total energy. An examination of the plot of the interaction energy $V(x, y)$ in Figure 1 shows that the system has two possible ground states: i) a state where the particles are grouped together into one block (minimal separation), and ii) a state where the particles are separated into clumps separated by a distance L. These two states correspond to the minima of the interaction potential $V(x, y)$, see Figure 1.

On the other hand, in the infinite temperature limit, the equilibrium state corresponds to the maximum of the entropy, which is given by the uniform density state studied in the previous section. This state is unique. Therefore, as the temperature is lowered, we expect that at some critical temperature we have a bifurcation (or transition) where the system condenses into one of the two ground states, or into a combination of them.

The situation is very similar to that encountered in the OSC model [19] which is also a model of one-dimensional gravitation, in a uniform background of mass, and with periodic boundary conditions. The treatment of the periodic boundary conditions is different, and results in a non-trivial external potential $\Phi(x)$. The Hamiltonian of this model is

$$H_{\rm OSC} = \sum_{i=1}^{N} \frac{1}{2} m v_i^2 + g m^2 \sum_{i>j} |x_i - x_j| - g m \bar{\rho} \sum_{i=1}^{N} \left[\left(x_i - \frac{1}{2} L \right)^2 + \frac{1}{4} L^2 \right] . \qquad (20)$$

Each particle feels the potential interaction with the uniform background $\Phi(x) = -gm\bar{\rho}[(x - \frac{1}{2}L)^2 + \frac{1}{4}L^2]$ which has the effect of pushing the particles towards the ends of the box $x \to 0$ and $x \to L$. The combined effect of the linear attraction potential, and of the external potential $\Phi(x)$ is to produce a complex phase diagram, with several phase transitions.

IV. SOLUTION OF THE MODEL

We derive in this Section the exact result for the thermodynamical properties of the system in the canonical ensemble, for arbitrary temperature. First we simplify the problem by taking without any loss of generality the size of the box to be $L = 1$. The parameter L can be absorbed into a redefinition of the coordinate $x/L \to x$. Second, for notational simplicity we denote the rescaled temperature $T_V = T/m$ simply as T. We will convert back to T in Section 5, in order to compare the theoretical predictions with the numerical simulation.

A. Lane-Emden equation

The single particle distribution function is found by solving the Lane-Emden equation. The result is given by the following Proposition.

Proposition 1. *The single particle distribution function of the gas in thermodynamical equilibrium $\rho(x)$ with $x \in [0,1]$ satisfies the Lane-Emden equation*

$$\frac{d^2}{dx^2}\log\rho(x) = 2\beta(1-\rho(x)) \tag{21}$$

normalized as

$$\int_0^1 dx\rho(x) = 1\,. \tag{22}$$

Proof. The functional $f_Q[\rho]$ for the configurational contribution to the free energy per particle (12) can be written as

$$f_{\rm Q}[\rho] = \inf_\rho \left\{ \frac{1}{2}g^2 \int_0^1 dxdy\rho(x)\rho(y)\left(|x-y| - (x-y)^2 - \frac{1}{6}\right) \right. \tag{23}$$
$$\left. + T\int_0^1 dx\rho(x)\log\rho(x) - T\log L \right\}$$

where we introduced $g^2 = 2\pi GML$. The function $\rho(x)$ appearing in this expression is a rescaled density and is related as $\rho(x) = L\tilde{\rho}(xL)$ where $\tilde{\rho}(y)$ is the density appearing in (12). For simplicity we assume in the remainder of the paper that the Boltzmann constant is $k_B = 1$. At equilibrium the free energy is minimal. We would like to minimize F under the constraint (22). This constraint can be taken into account by introducing a Lagrange multiplier λ and considering the functional $G[\rho] = f_Q[\rho] + \lambda(\int_0^1 dx\rho(x) - 1)$.

This variational problem gives the Euler-Lagrange equation for the gas density $\rho(x)$.

$$\frac{\delta}{\delta\rho(x)}G[\rho] = g^2\int_0^1 dy\rho(y)\left(|x-y| - (x-y)^2 - \frac{1}{6}\right) + T(\log\rho(x)+1) + \lambda = 0 \tag{24}$$

This integral equation can be transformed into a differential equation by taking 2 derivatives with respect to x. Writing explicitly the first integral, the Euler-Lagrange equation is written as

$$g^2\left(\int_0^x dy\rho(y)(x-y) + \int_x^1 dy\rho(y)(y-x) - \int_0^1 dy\rho(y)(x-y)^2 - \frac{1}{6}\right) \tag{25}$$
$$+T(\log\rho(x)+1) + \lambda = 0\,.$$

Taking one derivative with respect to x we get

$$g^2\left(\int_0^x dy\rho(y)-\int_x^1 dy\rho(y)-2\int_0^1 dy\rho(y)(x-y)\right)+T\frac{d}{dx}\log\rho(x)=0\,. \tag{26}$$

Take a second derivative

$$2g^2\rho(x)-2g^2+T\frac{d^2}{dx^2}\log\rho(x)=0 \tag{27}$$

This is the Lane-Emden equation (21), which holds for the single particle distribution function for a gas at temperature T [37]. This concludes the proof of this relation.

We would like to solve the equation (21) with the constraint (22), for given temperature T. It is convenient to introduce the new unknown function $y(x)$ defined by

$$\rho(x)=e^{y(x)} \tag{28}$$

Expressed in terms of this function, the differential equation (21) reads

$$y''(x)=2\beta g^2(1-e^{y(x)}) \tag{29}$$

with the normalization constraint

$$\int_0^1 dxe^{y(x)}=1\,. \tag{30}$$

We impose periodic boundary conditions

$$y(0)=y(1)\,,\qquad y'(0)=y'(1)\,. \tag{31}$$

We note that the equation (29) is identical to equation (12) in [19] (up to the redefinition $y(x)\to-\beta\psi(x)$ and rescaling $x/L\to x$), giving the density of the gas in the OSC model. However our boundary conditions (31) are more constraining than the boundary condition in [19]. In particular, we require $y(0)=y(1)$, which is not imposed in [19]. As a result, although the qualitative properties of the solution are similar in both cases, the details of the solution are different.

Remark 1. *We note that the normalization constraint (22) is automatically satisfied with the boundary condition $y'(0)=y'(1)$. Indeed, using the equation (29) we have*

$$\int_0^1 dxe^{y(x)}=\int_0^1 dx\left(1-\frac{1}{2\beta g^2}y''(x)\right)=1-\frac{1}{2\beta g^2}(y'(1)-y'(0))=1\,. \tag{32}$$

We write the equation (29) in the form

$$y''(x)=-V'(y(x))\,,\quad V(y)=\alpha^2(e^y-y-1) \tag{33}$$

where we defined $\alpha^2 = 2\beta g^2$. This has same form as the Newton's equation of motion for a particle of mass 1 in the potential $V(y)$. The total energy is conserved

$$E = \frac{1}{2}[y'(x)]^2 + \alpha^2(e^{y(x)} - y(x))\,. \tag{34}$$

Using this dynamical analogy it is easy to understand the qualitative behavior of the solutions of the differential equation (33). The equation (33) has always the trivial solution $y(x) = 0$, which corresponds to the particle sitting at rest at the bottom of the potential $V(y)$. In addition to this trivial solution it can have oscillatory solutions, corresponding to the particle moving in the potential $V(y)$, starting at some non-zero value $y(0) \neq 0$ with a positive or negative initial speed $y'(0)$, and then performing one full oscillation or several oscillations before returning to the starting point $y(1) = y(0)$ with the same velocity $y'(1) = y'(0)$ at time 1. The movement of the particle is spanned by $y_L \leq y(x) \leq y_R$, where $y_L < 0, y_R > 0$ are the turning points at which the particle speed vanishes. They are related by energy conservation to the initial position and speed as $V(y_L) = \frac{1}{2}[y'(0)]^2 + V(y(0)) = V(y_R)$. It is easy to see that one can take $y'(0) = 0$ without any loss of generality, as the solutions with non-zero $y'(0)$ are related to those with $y'(0) = 0$ by a translation.

We will be seeking solutions of the equation (33) with boundary conditions $y(0) = y(1), y'(0) = y'(1) = 0$ corresponding to the particle starting at rest at time 0 at $y(0)$ and returning to the same position at time 1. There are two solutions which are distinguished by the sign of the initial position: $y^{(+)}(0) > 0$ and $y^{(-)}(0) > 0$. However, it is easy to see that they are related by a translation $x \to x + C$, and it is sufficient to determine only one of them. We will choose as the representative solution the solution with $y(0) < 0$. From this one can generate a continuous family of solutions by translations in the x coordinate.

The solution $y(x)$ is given implicitly by

$$x = \int_{y(0)}^{y(x)} \frac{dy}{\sqrt{2\alpha^2(y - e^y - y(0) + e^{y(0)})}} \tag{35}$$

where $y(0)$ is a solution of the equation

$$2kt(y_0, \alpha) = 1\,, \qquad k = 1, 2, \cdots \tag{36}$$

$t(y_0, \alpha)$ is the time it takes the particle to move from $y_0 < 0$ when starting at rest $y'(0) = 0$, to the turning point with opposite sign $y_R(y_0)$. This function is given by

$$t(y_0, \alpha) = \frac{1}{\sqrt{2\alpha^2}} \int_{y_0}^{y_R(y_0)} \frac{dy}{\sqrt{y - e^y - y_0 + e^{y_0}}} \equiv \frac{1}{\sqrt{2}\alpha} F(y_0)\,, \tag{37}$$

with $y_R(y_0) > 0$ the positive solution of the equation $e^{y_0} - y_0 = e^{y_R(y_0)} - y_R(y_0)$. We defined the function $F(y_0)$ as the integral appearing in this expression. The plot of $F(|y_0|)$ is shown in Figure 2. It has the limiting value $\lim_{y_0 \to 0} F(y_0) = \sqrt{2}\pi$, and it is an increasing function of $|y_0|$.

The solutions of the equation (36) with $k = 1$ describe trajectories where the particle performs one full oscillation before returning to $y(0)$ at $x = 1$, the solutions with $k = 2$ give trajectories with two oscillations and so on. Equation (36) has both positive and negative solutions for y_0. As discussed above, it is sufficient to consider only the $y_0 < 0$ solution. We will denote the solution corresponding to given k as $y_k(x)$ and will call it the $k - th$ mode.

It is clear that the equation (36) has solutions for given $k \in \mathbb{N}$ only if $\frac{2\pi k}{\alpha} > 1$. In particular, for $\alpha < 2\pi$ this equation does not have a non-zero solution for y_0, and the only solution of the equation of motion (33) is the trivial solution $y(x) = 0$. For $2\pi < \alpha < 4\pi$ there is solution $k = 1$, for $4\pi < \alpha < 6\pi$ there are two solutions with $k = 1, 2$, and so on. We give in Table III a tabulation of the $k = 1$ solutions of the equation (36) for values of $\alpha > 2\pi$.

The higher order solutions are related to the $k = 1$ solution as

$$y_1(x, \alpha) = y_2\left(\frac{1}{2}x, 2\alpha\right) = \cdots = y_k\left(\frac{1}{k}x, k\alpha\right) . \tag{38}$$

It is easy to check by direct substitution into the equation $y''(x, \alpha) = \alpha^2(1 - e^{y(x,\alpha)})$ that these are indeed solution of this equation. In particular, this gives a relation among the solutions of the equation (36) with different values of k: $y_1(0, \alpha) = y_2(0, 2\alpha) = \ldots$.

For sufficiently small oscillation amplitude $|y_0| \ll 1$ the function $t(y_0)$ is given by the approximative formula

$$t(y_0) = \frac{\pi}{\alpha}\left(1 + \frac{1}{24}y_0^2 + O(y_0^4)\right) . \tag{39}$$

This follows from the expansion of the oscillation period for an anharmonic potential with small amplitude, see [39] for a detailed discussion and references to the literature. The small amplitude region $|y_0| \ll 1$ corresponds to α just above 2π (for $k = 1$), just above 4π (for $k = 2$), etc.

Using this approximation we get the solution of (36) for values of α around the critical value 2π

$$y_0^2 \simeq \begin{cases} 0 & , \alpha \leq 2\pi \\ 24\left(\frac{\alpha}{2\pi} - 1\right) & , \alpha > 2\pi \end{cases} \tag{40}$$

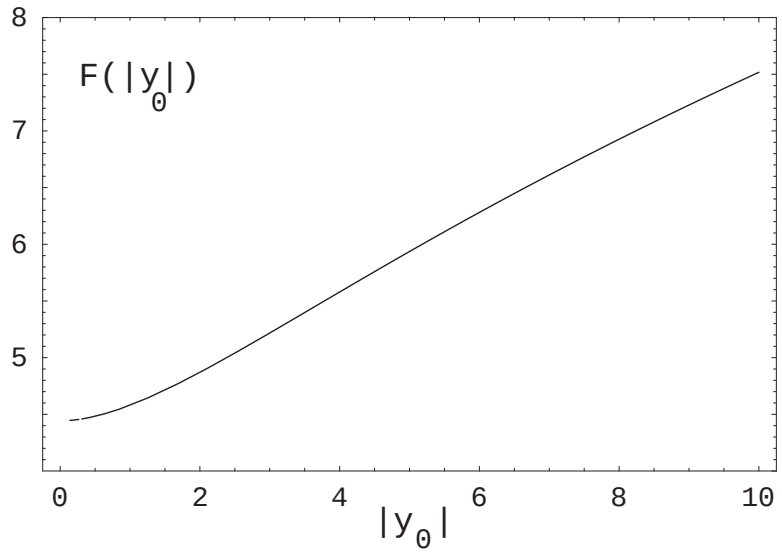

FIG. 2. Plot of the function $F(y_0)$ defined in (37) for $y_0 < 0$ vs $|y_0|$.

A similar formula gives $y_k(0)$ for α slightly above $2\pi k$ with $k = 2, 3, \cdots$. This is $y_k^2(0) \simeq 24(\frac{\alpha}{2\pi k} - 1)$.

For $|y_0| \ll 1$ we can find also an explicit approximative solution of the equation (35). This is given for $k = 1$ by

$$y_1(x) = y_1(0)\cos(2\pi x) \tag{41}$$

This follows by expanding the exponentials in the denominator of the integrand in a Taylor series to second order, which gives

$$x = \frac{1}{\alpha}\int_{y_0}^{y(x)} \frac{dy}{\sqrt{y_0^2 - y^2}} = \arccos\left(\frac{y(x)}{y_0}\right) . \tag{42}$$

The properly normalized density of the gas is $\rho(x) = \frac{1}{I_0(y_1(0))} e^{y_1(0)\cos(2\pi x)}$.

Combining (41) with (38) one can obtain also approximative solutions for $y_k(x)$ for α slightly larger than $2\pi k$.

The analysis presented above gives the following qualitative behaviour of the gas density as the temperature is lowered. In the infinite temperature limit $T \to \infty$ we have $\alpha \to 0$ and the gas density is constant $\rho(x) = 1$. As the temperature is lowered, the density $\rho(x)$ remains constant until we reach $\alpha = 2\pi$ when one non-trivial solution for y_0 appears. This point corresponds to temperature

$$T_{c1} = \frac{g^2}{2\pi^2} = \frac{2\pi GML}{2\pi^2} . \tag{43}$$

Compared to the critical temperature in the OSC model [19], this is smaller by a factor of $\frac{1}{4}$. This is due to our boundary condition $y(0) = y(1)$ which is not imposed in [19]. However, the result for T_{c1} has the same dependence on model parameters as in the OSC model, see Eq. (11) in [20] which gives $T_{c1} = \frac{2g^2}{\pi^2}$ in our notations. Note that in this reference $2\pi G$ is denoted g.

As the temperature is lowered below this point, non-trivial solutions with inhomogeneous gas density appear. They are translated versions of the basic solution $\rho_1(x) = \exp(y_1(x))$. $\rho_1(x)$ has a maximum at $x = 1/2$. We show in Figure 3 typical results for the gas density profiles $\rho_1(x)$ for two values of $\alpha = 6.3$ (just above 2π) and $\alpha = 7$ (solid curves). These are compared with the approximation (41) (dashed curves) which is seen to work well for temperature just below the transition temperature T_{c1}.

As the temperature is lowered further, we reach the point $\alpha = 4\pi$, corresponding to temperature $T_{c2} = \frac{g^2 ML}{8\pi^2}$. Below this temperature there are two solutions for $y(x)$ corresponding to $k = 1, 2$. In addition to the $k = 1$ solution we have another solution with $k = 2$, which has oscillatory density behavior, and has two maxima/minima within the box. In general there is an infinite sequence of critical temperatures at which new solutions appear, given by $\alpha = 2n\pi$, with $n = 1, 2, \cdots$

$$T_{cn} = \frac{g^2}{2n^2\pi^2} = \frac{2\pi GML}{2n^2\pi^2}\,. \tag{44}$$

Note that we have not yet proven that these solutions of the Lane-Emden equation for the gas density $\rho(x)$ correspond to stable configurations of the gas. In order to decide which solutions are stable one has to compare their free energy and determine the solution which minimizes the free energy. This will be done in the next section.

B. Thermodynamics

We discuss next the thermodynamical properties of the system. They can be obtained from the free energy F, which is given by the following result.

Proposition 2. *The free energy per particle of the gas is given by*

$$\frac{F}{N} = \frac{1}{2g^2}T^2 \int_0^1 dx[y'(x)]^2 + T(1 - e^{y_0} + y_0) - T\log L + f_{\rm kin}\,, \tag{45}$$

where $y_0 < 0$ is the solution of the equation $\sqrt{\frac{2}{\alpha}}F(y_0) = 1$ with $F(y_0)$ defined in (37). The contribution from the kinetic degrees of freedom is $f_{\rm kin} = T(\log N - 1 + \frac{1}{2}\log\frac{h^2}{2\pi T})$. The

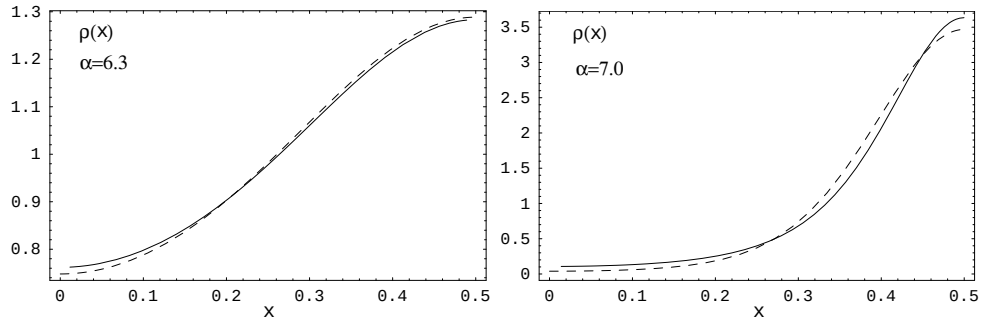

FIG. 3. Plots of the density $\rho(x)$ vs x for several values of $\alpha^2 = 2\beta g^2$ (solid curves). The dashed curves show the approximation (41) which is valid for $\alpha \sim 2\pi$. Left: $\alpha = 6.3$, right: $\alpha = 7$.

integral in the first term depends only on $\alpha^2 = 2g^2\beta$ *and is given explicitly for the* $k-th$ *solution of the equation (36) as*

$$K_k(\alpha) \equiv \int_0^1 dx[y_k'(x)]^2 = 2k \int_{y_0}^{y_R(y_0)} dx\sqrt{2\alpha^2(x - e^x - y_0 + e^{y_0})} \tag{46}$$

Recall that $y_R(y_0) > 0$ *is the unique positive solution of the equation* $e^{y_0} - y_0 = e^{y_R(y_0)} - y_R(y_0)$ *with* $y_0 < 0$. *This is the turning point in the equivalent dynamical interpretation of the equation satisfied by* $y(x)$.

Proof. See Appendix B.

We note that in the $T \to \infty$ limit, we have $\alpha \to 0$ and the free energy (45) reduces to the free energy of the uniform gas which is given in (18).

For α slightly above 2π (corresponding to temperature T just below the first critical point T_{c1}), we can derive a closed form approximation for the function $K_1(\alpha)$ by expanding the exponential function in the integrand. This gives

$$K_1(\alpha) = 2\alpha y_0^2 \int_{-1}^{1} dx\sqrt{1 - x^2} = \pi\alpha y_0^2 \,. \tag{47}$$

We study the behavior of the free energy around the critical point T_{c1}. The free energy per particle is

$$f = f_0 + \frac{1}{2g^2} T^2 K_1(\alpha) + T(1 - e^{y_0} + y_0) \tag{48}$$

where $f_0 = T(\log(N/L) - 1 + \frac{1}{2}\log\frac{h^2}{2\pi T})$ is the free energy per particle in the homogeneous density phase, below the critical temperature.

Substituting here the approximations for $K_1(\alpha)$ and y_0^2 (47) and (40) we have, for α just above 2π

$$f - f_0 \simeq \frac{1}{2g^2} T^2 \pi \alpha y_0^2 + T(-\frac{1}{2} y_0^2) \tag{49}$$
$$= \frac{1}{2} T y_0^2 \left(\frac{2\pi}{\alpha} - 1 \right) = -\frac{24\pi T}{\alpha} \left(\frac{\alpha}{2\pi} - 1 \right)^2 .$$

Expressing α in terms of temperature as $\frac{\alpha}{2\pi} = \sqrt{\frac{T_{c1}}{T}}$ we have

$$f - f_0 \simeq -12 T_{c1} \sqrt{x} (1 - \sqrt{x})^2 \tag{50}$$

with $x \equiv T/T_{c1}$. It is easy to see that the free energy difference $f - f_0$ and its first derivative with respect to temperature vanish at $T = T_{c1}$, while the second derivative has a jump from 0 at $T > T_{c1}$ to $\lim_{T \to T_{c1} - 0} \partial_T^2 (f - f_0) = -6 T_{c1}$. Since the difference $f - f_0$ vanishes for $T > T_{c1}$, this implies that the free energy and its derivative are continuous at $T = T_{c1}$ while its second derivative has a jump. We conclude that the phase transition at $T = T_{c1}$ is a second order phase transition.

We study further the properties of the system around the critical temperature T_{c1}. The energy per particle of the gas is given by (14). This can be written in a more explicit way as

$$u = \frac{1}{2} T - \frac{1}{4g^2} T^2 \int_0^1 dx [y'(x)]^2 . \tag{51}$$

The first term is the kinetic energy contribution, which is given by the equipartition theorem as $\frac{1}{2} k_B T$ per particle. The second term is the contribution of the interaction energy, which can be expressed in this form using the Lane-Emden equation as shown in Appendix B

$$\frac{1}{2} (2\pi G M L) \int_0^1 dx dy \rho(x) \rho(y) (|x - y| - (x - y)^2 - \frac{1}{6}) = -\frac{1}{2} T J - \frac{1}{2} (\lambda + T) \tag{52}$$

The integral $J = \int_0^1 dx \rho(x) \log \rho(x)$ and Lagrange multiplier λ are given explicitly in Appendix B. Substituting their expressions here gives the result (51).

For temperature above the critical temperature, the gas density is uniform and the contribution of the interaction energy vanishes. The energy per particle is due in this region only to the kinetic degrees of freedom. Below the critical temperature, the gas becomes non-uniform and the interaction energy starts to contribute a non-vanishing amount.

We compute next the specific heat per particle. This can be obtained by taking a derivative of (51) with respect to the temperature and is given by

$$c_V = \left(\frac{\partial u}{\partial T}\right)_L = \frac{1}{2} + \frac{1}{8\pi}\sqrt{\frac{T}{T_{c1}}}K_1'(\alpha) - \frac{1}{4\pi^2}\frac{T}{T_{c1}}K_1(\alpha) = \frac{1}{2} + 3F_{c_V}(\alpha)\,, \tag{53}$$

where we defined

$$F_{c_V}(\alpha) \equiv \frac{1}{12\alpha}K_1'(\alpha) - \frac{1}{3\alpha^2}K_1(\alpha) \tag{54}$$

This was obtained by writing $\alpha = 2\pi\sqrt{T_{c1}/T}$ and using (43). For temperatures just below T_{c1} we can approximate $K_1(\alpha)$ using (47). Using this approximation we have $\lim_{\alpha\to 2\pi} K_1(\alpha) = 0\,, \lim_{\alpha\to 2\pi} K_1'(\alpha) = 24\pi$, which gives

$$\lim_{\alpha\to 2\pi} F_{c_V}(\alpha) = 1\,. \tag{55}$$

This implies that the specific heat is discontinuous at the critical point. Above the critical point T_{c1} the specific heat is constant and equal to $c_V = \frac{1}{2}$, and below the critical point it takes the value

$$\lim_{T\to T_{c1}-\epsilon} c_V = 3 + \frac{1}{2} = \frac{7}{2}\,. \tag{56}$$

We can obtain an approximation for the temperature dependence of the specific heat per particle $c_V(T)$ below the critical temperature, using the approximation (47) for the function $K_1(\alpha)$. This gives the following approximation for $F_{c_V}(\alpha)$ defined in (54), valid for $\alpha - 2\pi \ll 1$

$$F_{c_V}(\alpha) \simeq \frac{6\pi}{\alpha} - 2\,. \tag{57}$$

The corresponding result for the specific heat per particle ia

$$c_V(T) \simeq \frac{1}{2} + 3(3\sqrt{T/T_{c1}} - 2)\,. \tag{58}$$

We show in Figure 4 the plot of the specific heat $c_V(T)$ vs T/T_{c1}. The solid curve is the exact result (53), and the dashed curve shows the approximative result (58).

C. The higher modes

The properties of the $k \geq 2$ modes can be related to those of the $k = 1$ mode. This implies that it is sufficient to study the solution of the system for the $k = 1$ mode. This is given by the following relations.

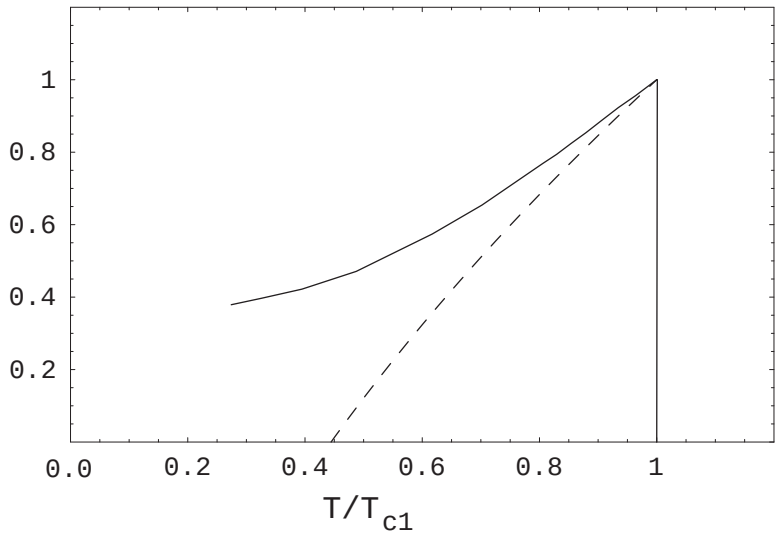

FIG. 4. Plot of the specific heat per particle $\frac{1}{3}(c_V(T) - \frac{1}{2})$ vs T/T_{c1}. This is the excess of the specific heat over the constant value $\frac{1}{2}$ which it takes in the homogeneous phase (times 1/3). The specific heat has a finite jump at T_{c1}. The solid curve shows the exact result (53) and the dashed curve shows the approximation (58) valid near the critical point.

Proposition 3. *The solutions of the equation (36) are related as*

$$y_k(0,\alpha) = y_1(0, \frac{1}{k}\alpha) \tag{59}$$

and the integrals (46) are related as

$$K_k(\alpha) = k^2 K_1(\frac{1}{k}\alpha) \tag{60}$$

For simplicity, we prove these relations for $k = 2$. The generalization to arbitrary $k \geq 2$ is immediate. These relations follow from equation (38). For $k = 2$ this gives $y_2(x, 2\alpha) = y_1(2x, \alpha)$. Taking here $x = 0$ gives the first identity (59). The second identity (60) is proved as

$$\begin{aligned} K_2(2\alpha) &= \int_0^1 dx[y_2'(x,2\alpha)]^2 = 2\int_0^{1/2} dx[y_2'(x,2\alpha)]^2 = 8\int_0^{1/2} dx[y_1'(2x,\alpha)]^2 \\ &= 4\int_0^1 dx[y_1'(x,\alpha)]^2 = 4K_1(\alpha) \end{aligned} \tag{61}$$

D. Stability analysis

The difference between the free energy of the $k-$th mode and of the uniform density state ($k=0$) is obtained by taking the difference of (45) and (18). This can be written as

$$\Delta f_k \equiv f(y_k(x)) - f_0 = T\left(1 - e^{y_0} + y_0 + \frac{1}{\alpha^2}K_k(\alpha)\right) \equiv T\delta_k(\alpha) \tag{62}$$

where we defined $\delta_k(\alpha)$. This function has a simple interpretation in terms of the dynamical analogy of the anharmonic oscillator discussed above.

Remark 4. *The function $\delta_k(\alpha)$ is related to the classical action along the trajectory of the equivalent dynamical system discussed above as*

$$\mathcal{S}[y(x)] = \int_0^1 dx \left[\frac{1}{2}[y'(x)]^2 - \alpha^2(e^{y(x)} - y(x))\right] . \tag{63}$$

It is easy to see that we have

$$\delta_k(\alpha) = 1 + \frac{1}{\alpha^2}\mathcal{S}[y_k(x)] . \tag{64}$$

The function $\delta_k(\alpha)$ is tabulated numerically for the first two modes in Table III in Appendix B. From these results one observes that $\Delta f_{1,2}$ is negative for temperatures below T_{c1} corresponding to $\alpha > 2\pi$. We prove next this result analytically for $k=1$.

For temperatures just below the first critical temperature T_{c1} the free energy difference of the $k=1$ mode is given approximatively by

$$\delta_1 = \frac{1}{2}\pi T\alpha y_0^2 + 1 - e^{y_0} + y_0 \simeq 1 - e^{y_0} + y_0 + \pi T\sqrt{\frac{T}{2\bar{\rho}}}y_0^2 \tag{65}$$

where we used the approximation (47) which is valid for $|y_0| \ll 1$, just below the first critical temperature T_{c1}. This is written equivalently as

$$\delta_1 \simeq 1 - e^{y_0} + y_0 + \frac{1}{2}T\sqrt{\frac{T}{T_{c_1}}}y_0^2 \leq 1 - e^{y_0} + y_0 + \frac{1}{4\pi^2}y_0^2 \tag{66}$$

where we used $T < T_{c1}$.

It is easy to see that the function $f(x) = 1 - e^x + x + \frac{1}{4\pi^2}x^2$ is strictly negative for any $x \neq 0$. This can be seen either by explicit numerical evaluation or can be proved analytically as follows. For $x > 0$ it follows from the inequality $e^x \geq 1 + x + \frac{1}{2}x^2$ (which is valid for $x \geq 0$), and for $x < 0$ it follows from the inequality $e^x \geq 1 + x^2/2$ (which is valid for any real x). We have proven thus that the first mode $y_1(x)$ is a stable equilibrium state for the gas

at temperatures just below the first critical temperature $T < T_{c1}$. The gas density becomes inhomogeneous in this region, and has a unimodal shape with a maximum or minimum at the center of the box.

Next we study the stability of the higher modes. Proposition 4 implies the following result

$$\delta_k(k\alpha) = \delta_1(\alpha) \tag{67}$$

This shows that it is sufficient to compute the free energy of the $k = 1$ mode and we obtain automatically also the free energies of the higher modes. For example these relations give $\delta_2(2\alpha) = \delta_1(\alpha)$, which can be checked to hold indeed on the numerical results in Table III.

Numerical calculation of $\delta_1(\alpha)$ shows that it is a monotonously decreasing function of α, which is zero at $\alpha = 2\pi$ and decreases to larger and larger (in absolute value) negative values as α increases. The relation (67) implies that the $k = 1$ mode has the lowest free energy at all temperatures below the first critical point $T < T_{c1}$. The higher modes $k \geq 2$, when they exist (for temperatures below the corresponding critical temperatures) are unstable minima of the free energy, and the system will always relax into a $k = 1$ state.

V. NUMERICAL SIMULATION

We present in this Section the results of a numerical simulation of the model. The simulation solved numerically the dynamical equations of motion of N particles interacting by the potential (4). Since the dynamical behavior of the system only depends on the net gravitational field experienced by the gravitating sheets (henceforth referred to as "particles" or "bodies"), we drop the constant term in the potential energy for simplicity. Hence, the potential energy for a system with primitive cell of length L and containing N particles may be expressed as

$$V = -2\pi G m^2 \sum_{j=2}^{N} \sum_{i=1}^{j-1} \left(\frac{(x_j - x_i)^2}{L} - |x_j - x_i| \right), \tag{68}$$

where x_i and x_j represent the primitive-cell positions of the i-th and the j-th particles respectively, with $x \in [-L/2, L/2)$. It should be noted that Miller and Rouet considered an "expanding-universe" version of the gravitational system whereby the positions of the particles were expressed in comoving spatial coordinates. Equations of motion were derived and it was shown that the choice of comoving coordinates invoked a damping factor in

the equations of motion. The exact evolutions of each particles' positions and velocities were implicit in the derived equations of motion. However, expressions for the time dependence were not explicitly provided. Here, for the sake of completion, we provide the time-dependencies in fixed (non-comoving) coordinates and discuss the evolution algorithm briefly.

Following Ref. [14] for non-comoving spatial coordinates, it can be shown for an ordered system $(x_1 < x_2 < \ldots < x_N)$ that

$$\frac{d}{dt}W_j(t) = \frac{d^2}{dt^2}Z_j(t) = 2\pi mG\left\{\frac{2N}{L}Z_j(t) - 2\right\}, \tag{69}$$

where v_j is the velocity of the j-th particle, $Z_j \equiv (x_{j+1} - x_j)$, and $W_j \equiv (v_{j+1} - v_j)$. Solutions to Eq. (69) provide the displacements and velocities of $(j+1)$-th particle with respect to those of j-th particle in between events of interparticle crossing:

$$Z_j(t) = \frac{L}{N} + \frac{1}{2}\left\{Z_j(0) - \frac{L}{N} + \frac{W_j(0)}{\Lambda}\right\}e^{\Lambda t} + \frac{1}{2}\left\{Z_j(0) - \frac{L}{N} - \frac{W_j(0)}{\Lambda}\right\}e^{-\Lambda t}, \tag{70}$$

$$W_j(t) = \frac{\Lambda}{2}\left\{Z_j(0) - \frac{L}{N} + \frac{W_j(0)}{\Lambda}\right\}e^{\Lambda t} - \frac{\Lambda}{2}\left\{Z_j(0) - \frac{L}{N} - \frac{W_j(0)}{\Lambda}\right\}e^{-\Lambda t}, \tag{71}$$

where $\Lambda \equiv \sqrt{\frac{4\pi mGN}{L}}$.

Crossing times, t_{c_j} may be obtained analytically as the smaller positive root (out of the two possible real ones) of $Z_j(t_{c_j}) = 0$. We find the crossing times using an event-driven algorithm similar to ones discussed in Refs. [14, 15]. The algorithm keeps track of the evolution by assigning an identifying label to each particle. Once a crossing occurs, the algorithm interchanges the labels and the velocities of the two participating particles at the crossing location. In the following iteration, the algorithm treats the updated system as a new, ordered one but maintains the original labels, thereby allowing for correct tracking of each particle's position and velocity. At the end of each iteration, positions x_j and velocities v_j are obtained respectively from Z_j and W_j by utilizing the contraints set forth by the conservation of momentum on the position and velocity of the center of mass [15].

In the simulation, we adopt a set of dimensionless units and rescale the system parameters as follows: $2\pi G = 0.5$, the total mass per unit cell, $mN = 1$, and the unit-cell size, $L = 1$. Consequently, the characteristic frequency of the system, $\Lambda = 1$. Without losing generality, we set the initial velocity of the center of mass to zero.

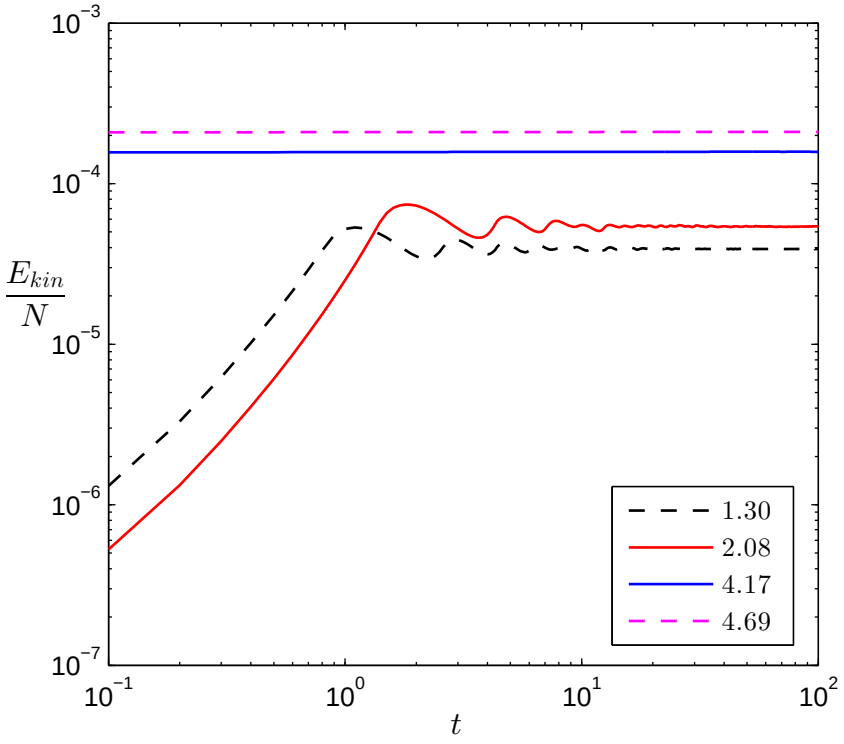

FIG. 5. Illustration of convergence of kinetic energy per particle in simulation for the first 100 time units out of a total time of 1200. The numbers in the legend represent the value of $\frac{U}{N}(\times 10^{-4})$.

With the ability to follow the exact time evolution, we study the thermodynamic behavior of the system for different values of N and, for each N, with varying per-particle energy. For the system to exhibit ergodic-like behavior, we avoid low values of N [22], i.e., we choose $N \geq 20$. A molecular-dynamics approach then predicates that the time-averaged values of the thermodynamic quantities will converge to those in the thermodynamic limit when N becomes sufficiently large.

A. Kinetic energy

Per-particle kinetic energies (E_{kin}/N) have been found by sampling the velocities at fixed intervals and averaging the per-particle kinetic energies from each interval over a sufficiently long time. The simulation are first run for $t = 1200$, and if the standard deviation σ_{kin} from the last 200 time units have converged to within a set tolerance with respect to the average value, the simulation is terminated. Otherwise, the simulation is allowed to run until the last

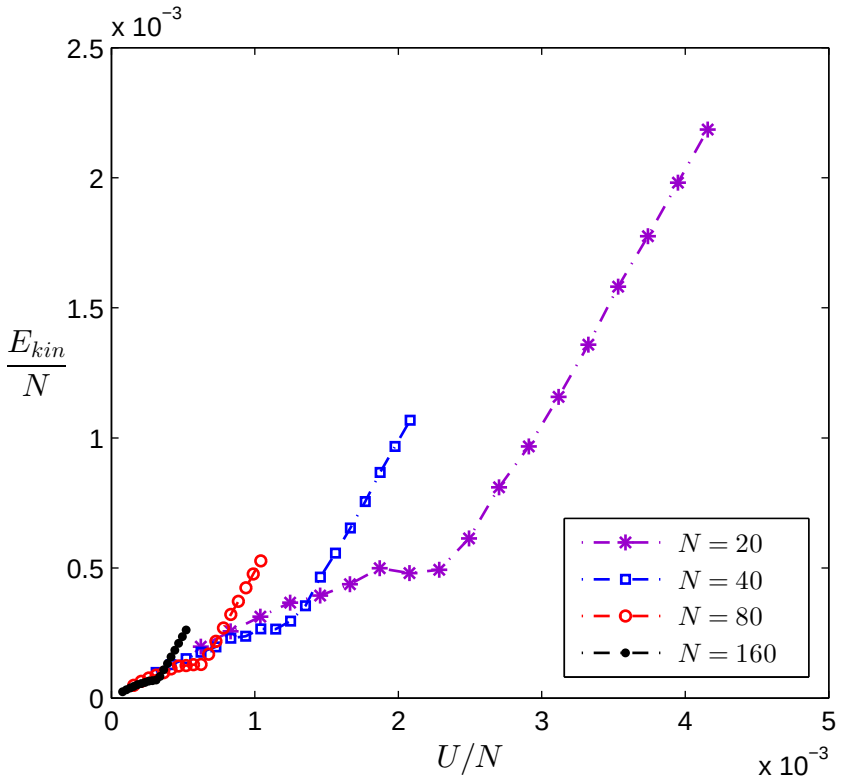

FIG. 6. Per-particle kinetic energy plotted against per-particle energy for varying number of particles.

200 time units produce a standard deviation smaller than the tolerance. In our simulations, we specified a tolerance of 1 percent, that is, $\sigma_{kin} \leq (0.01 \times E_{kin}/N)$.

Figure 5 shows the evolution of E_{kin}/N for the first 100 time units out of a total evolution time of $t = 1200$ at four different values of per-particle energy U/N for a system with $N = 160$. Table I shows the converged value of E_{kin}/N for the same four energies and the corresponding values of σ_{kin} relative to E_{kin}/N. Evidently, if the value of U/N exceeds the maximum allowed per-particle potential energy, the system acts as an ideal gas and average values ofE_{kin}/N converges very rapidly. On the other hand, at energies lower than than maximum allowed values, the system goes through a relaxation phase before the time-averaged values of E_{kin}/N converge.

Figure 6 shows the caloric curves, E_{kin}/N versus U/N, for $N = 20, 40, 80$, and 160. Although a transitioning trend is observed for each N, the results indicate that the system approaches a "thermodynamic-limit" behavior at $N \sim 80$, that is, the transitions become

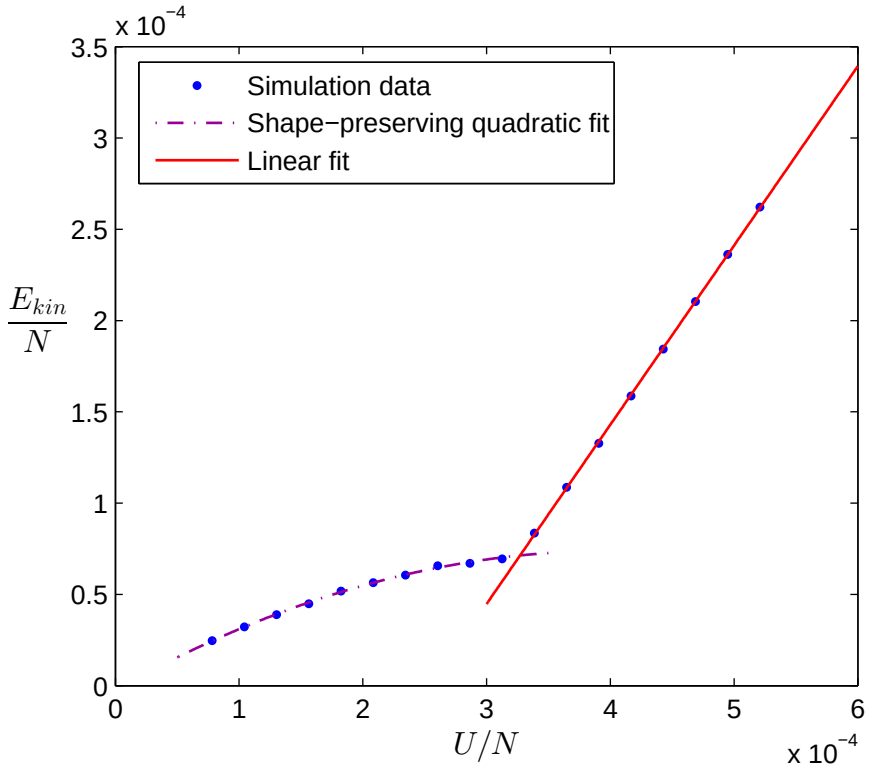

FIG. 7. Per-particle kinetic energy versus per-particle energy for $N = 160$. A clear-cut jump is evident in the first derivative of the caloric curve.

sharp for $N \geq 80$. The caloric curve for $N = 160$ has been reproduced separately in Fig. 7. A discontinuity in the first derivative is profoundly evident.

B. Radial distribution function

The radial distribution function, $g(r)$ encapsulates how the density varies with respect to distance r from a reference particle in a system. To calculate $g(r)$ in simulation, we employ the approach proposed in Ref. [15]. The positions of the particles are sampled at fixed time-intervals of $d\tau$. At the end of k-th interval (corresponding to time, $t = kd\tau$), we find the number of particles, $\Delta N_j(r,t)$ in a small volume (length) element Δr at a distance r from a reference particle at x_j. The radial distribution function is then found as

$$g(r) = \lim_{l\to\infty} \frac{\sum_{k=0}^{l} \sum_{j=1}^{N} \Delta N_j(r, t = kd\tau)}{(2\Delta r) N l \bar{\rho}}, \tag{72}$$

where l is the number of iterations and $\bar{\rho} = N/L$. Note that, in Ref. [15], the bulk number-density, $\bar{\rho}$ was chosen to be unity, and hence, it was not included in the expression for $g(r)$. In our simulation, however, L has been set to unity, and therefore, $\bar{\rho}$ is simply equal to N.

For systems that are homogeneous (and isotropic, in case of two- or three-dimensional systems), $\bar{\rho}g(r)\mathrm{d}r$ represents the probability of observing a second particle in $\mathrm{d}r$ at a distance r provided a particle is located at $r = 0$ and $g(r) \to \frac{N-1}{N}$ for large r. [40]. However, in our case, the system remains essentially non-homogeneous at low energies and the time-averaged value of the density at a position $\mathbf{r}$ relative to any given particle at $\mathbf{r}_i$ is not equal to the space-averaged bulk density $\bar{\rho}$. That is, $\langle \rho(\mathbf{r} - \mathbf{r}_i) \rangle \neq \bar{\rho}$. Therefore, for low-energy configurations of the Miller-Rouet gravitational gas, $g(r)$ as expressed in Eq. (72) does not quite represent the standard definition of the radial distribution function as generally used in statistical mechanics. However, it still serves as a good indicator of the relative distribution of the particles with respect to one another. Figure 8 shows typical low-energy μ-space distributions and the corresponding plots of $g(r)$ at different values of elapsed time. It is evident that the particles tend to stay clumped together and the particle distribution is inhomogeneous.

At high energies, the particles are able to spread across the entire primitive cell and the distribution tends to be homogeneous. That is, $\langle \rho(\mathbf{r} - \mathbf{r}_i) \rangle \sim \bar{\rho}$ for $U > V_{max}$, where V_{max} represents the maximum allowed value of the potential energy for a given number of particles. Under such conditions, $g(r)$ as given in Eq. (72) represents the radial distribution function in the standard sense. Figure 9 shows a set of high-energy μ-space distributions

TABLE I. Converged values of kinetic energy per particle from simulation for $N = 160$ found at the four values of per-particle energies used in Fig. 5. In each case, the total simulation time was 1200 and the standard deviation σ_{kin} was calculated for the last 200 time units.

$\frac{U}{N}(\times 10^{-4})$	$\frac{E_{kin}}{N}(\times 10^{-4})$	$\frac{\sigma_{kin}}{(E_{kin}/N)}(\times 10^{-4})$
1.30	0.39	2.67
2.08	0.56	9.92
4.17	1.59	1.70
4.69	2.10	0.19

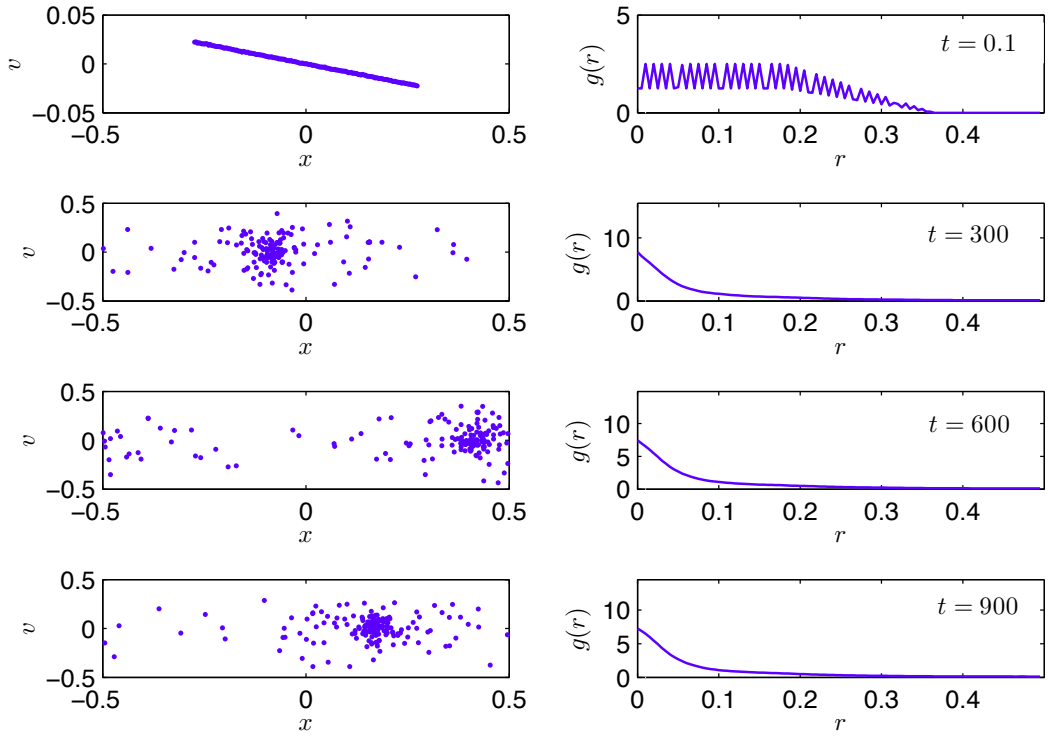

FIG. 8. μ-space snapshots (left column) and time-averaged values of the radial distribution function (right column) for $U/N = 2.08 \times 10^{-4}$ and $N = 160$ at different instants of time. Corresponding elapsed time for each row is mentioned in the $g(r)$ plot.

and the corresponding plots of $g(r)$ at different instants of time. Clearly, the distribution is more uniform in this case (as compared to Fig. 8) and $g(r)$ appears to approach the expected value of $\frac{159}{160}$ away from $r = 0$.

C. Pressure

The pressure has been calculated in simulation by following the method discussed in Ref. [15]. The method involves placing virtual walls at regular spatial intervals throughout the primitive cell and time-averaging the momentum transferred from hypothetical elastic collisions to each wall from a given direction (left or right side of the wall). The wall separation and the averaging time are decided by an adaptive algorithm that takes into account a user-provided tolerance as the convergence criterion.

Before we start calculating the pressure, the system is allowed to relax for $t = 1200$.

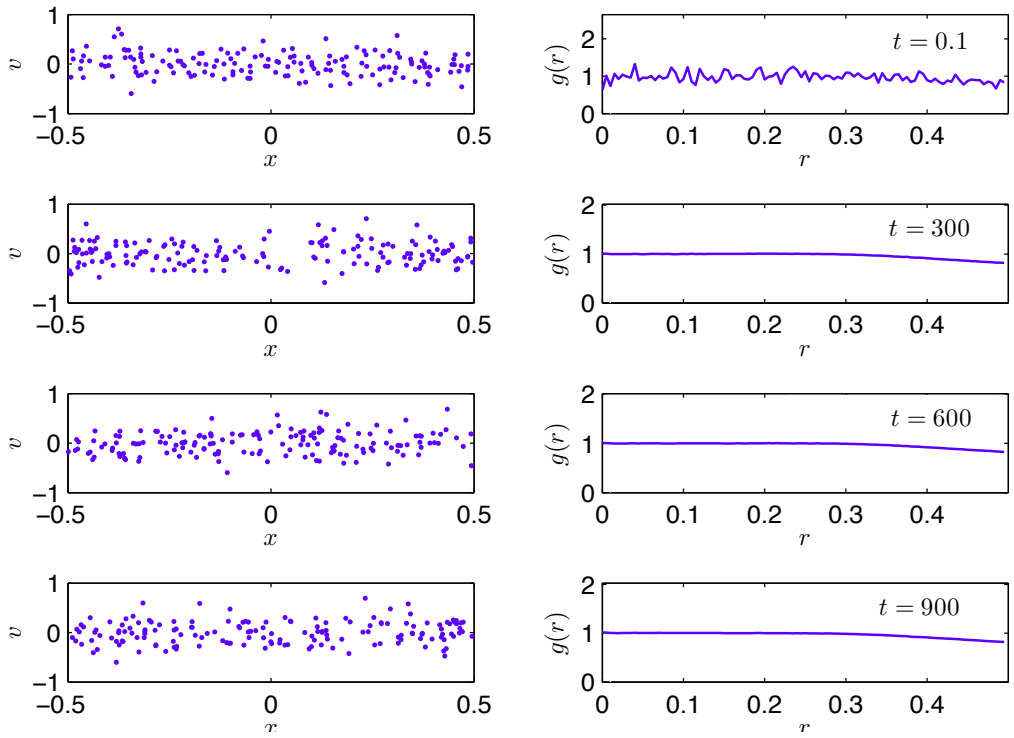

FIG. 9. μ-space snapshots (left column) and time-averaged values of the radial distribution function (right column) for $U/N = 4.17 \times 10^{-4}$ and $N = 160$ at different instants of time. Corresponding elapsed time for each row is mentioned in the $g(r)$ plot.

Positions and velocities after the initial run of 1200 time units are then used as initial conditions for the pressure routine. For energies greater than the maximum allowed potential energy in the system, the value of pressure converged fairly easily to within 1 percent in $t = 500$, with as few as 10 walls per unit length for $N = 160$. The relatively easy convergence may be attributed to the the fact that the behavior of the system resembles that of an ideal gas for energies greater than the critical value of U, However, for energies lower than that corresponding to the critical point, we had to increase the convergence tolerance to 5 percent for the adaptive algorithm to terminate eventually. At a 5-percent tolerance, convergence times varied between $t = 800$ and $t = 1400$ with 100 walls for $N = 160$ and energies below the critical value.

It should be noted that the particles are tightly coupled via potential at lower energies and the time evolutions of particles' positions and velocities are strongly exponential between events of crossings (as opposed to being uniform, "ideal-gas-like" for higher energies).

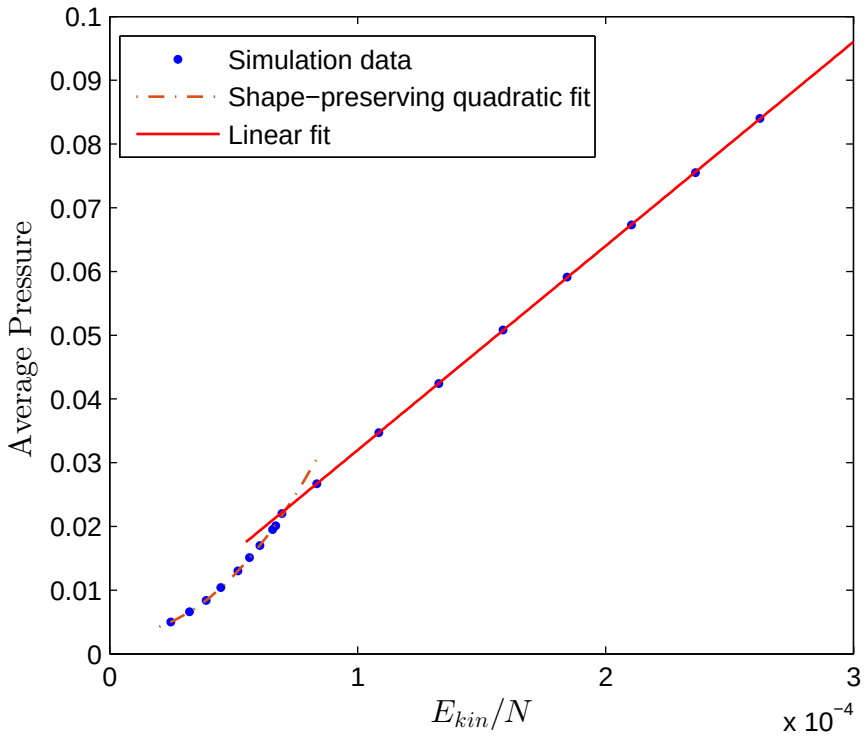

FIG. 10. Time-averaged pressure versus per-particle kinetic energy for $N = 160$.

Hence, at energies below the critical value, finding pressure as an average rate of momentum transferred by placing regularly-spaced virtual walls becomes a rather crude approximation. To counter the effect of the strong coupling on the accuracy of the results, one would have to put increasingly larger number of virtual walls as the energy gets closer to the critical value. However, the marginal increase in the accuracy from inserting additional walls diminishes drastically as the interactions get stronger, thereby making the simulation increasingly time-consuming for a given convergence tolerance. Nevertheless, as shown in Fig. 10, a 5-percent tolerance provided a fairly good handle on the temperature dependence of pressure for $N = 160$, and a clear-cut change in slope is displayed near the critical value of E_{kin}/N.

D. Largest Lyapunov exponent

The largest Lyapunov characteristic exponents (LCEs) have been calculated for $N = 160$ using the method discussed in Ref. [22]. Similar to the pressure algorithm, the LCE routine uses the positions and velocities from a prior relaxation run of 1200 time units as the initial

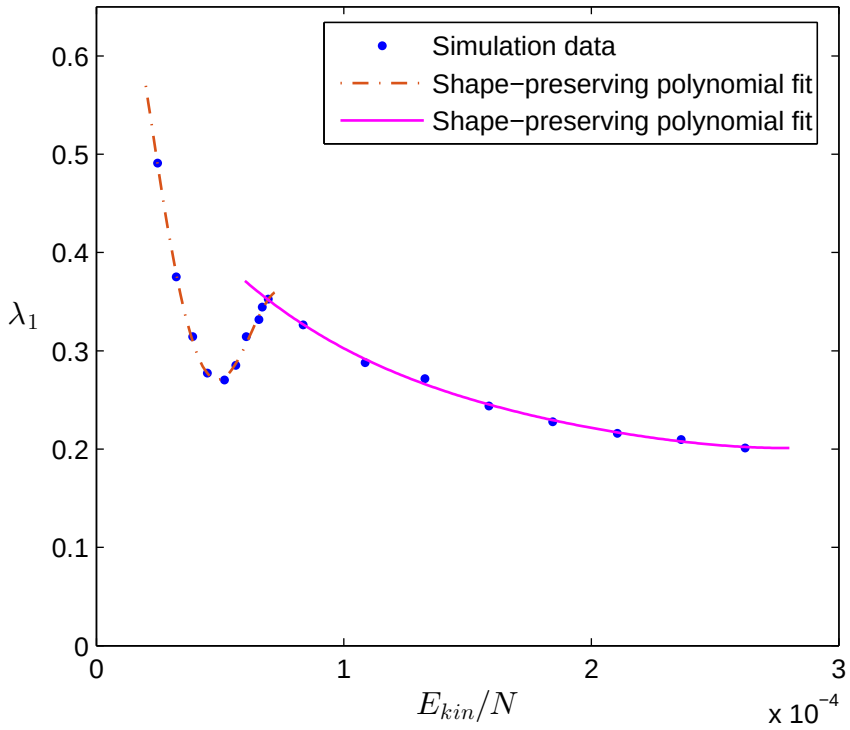

FIG. 11. Largest Lyapunov characteristic exponent versus per-particle kinetic energy for $N = 160$.

conditions. The program is adaptive in that it is allowed to run as long as the standard deviation of the largest Lyapunov exponent from the last 1 million crossings is greater than 1 percent of the average value, with a minimum of 4 million crossings. We found that the largest LCE for each U/N converged to within 1 percent in the first 4 million crossings. Results for $N = 160$ have been presented in Fig. 11. It can be seen from the figure that the largest LCE exhibits a local maximum as well as a discontinuity in the slope near the transition point.

VI. DISCUSSION

In this section, we compare the results of our simulation with those predicted by our theoretical treatment. We recall that the theoretical results are expressed in terms of the Vlasov rescaled temperature $T_V = T/m$. In order to compare with the simulation, we have to express the theoretical predictions in terms of the usual temperature $T = T_V m = T_V M/N$. We also express the energies (U and E_{kin}) in the rescaled units that were adopted in the

simulation.

The simulation used the following parameter values: interaction coupling $2\pi G = \frac{1}{2}$, total gas mass $M = mN = 1$ and gas volume (length of elementary cell) $L = 1$. Thus we have $g^2 = 2\pi GML = \frac{1}{2}$. Also, the constant term $g^2(-\frac{1}{6}L)$ in the potential (10) was not included in the simulation, and its effect has to be explicitly subtracted from the theoretical result.

A. Energy per particle

The total gas energy per particle is given by equation (14) which gives

$$u = U/N = \frac{1}{2}T_V - \frac{1}{2}T_V^2 \int_0^1 dx[y'(x)]^2 \tag{73}$$

In order to compare with the numerical simulation, the result (73) must be adjusted in two ways:

i) we must subtract the contribution of the constant term $-\frac{1}{6}$ in the interaction energy (14) which was not included in the simulation;

ii) we must multiply u with m, the particle masses, in order to account for the fact that we rescaled both the kinetic and interaction potential energies by one factor m.

We get thus the following theoretical prediction for the energy per particle in the simulation

$$\begin{aligned} u_{\rm sim} = \frac{U_{\rm sim}}{N} &= m(u + \frac{1}{24}) = \frac{1}{2}mT_V + \frac{1}{24}m - \frac{1}{2}mT_V^2 \int_0^1 dx[y'(x)]^2 \\ &= \frac{1}{2}T + \frac{M}{24N} - \frac{1}{2M}NT^2 \int_0^1 dx[y'(x)]^2 \end{aligned} \tag{74}$$

The second term is the contribution of the constant term $-\frac{1}{6}$ which was not included in the simulation. This is

$$\Delta U/N = \frac{1}{2}g^2 \int_0^1 dxdy\rho(x)\rho(y)\frac{1}{6} = \frac{1}{24}\,. \tag{75}$$

B. Critical temperature

The critical Vlasov temperature is given by equation (43). Taking into account the normalization factor $g^2 = \frac{1}{2}$ this is $(T_V)_{c1} = \frac{1}{4\pi^2}$. Converting to the actual temperature as $T = T_V m = T_V M/N$ we get the critical temperature

$$T_{c1} = \frac{1}{4\pi^2 N} \tag{76}$$

TABLE II. Numerical results for the kinetic energy per particle at the critical temperature, from equation (77), for the values of N considered in the simulation.

N	$\frac{1}{2}T_{c1}(\times 10^{-4})$
20	6.33
40	3.17
80	1.58
160	0.79

Thus we expect to see a discontinuity in the derivative of the caloric curve, defined as $u_{\rm sim}(T)$ with $u_{\rm sim}$ the total gas energy per particle, given in (74), at

$$\frac{E_{kin}}{N} = \frac{1}{2}T_{c1} = \frac{1}{8\pi^2 N} \tag{77}$$

We tabulated in Table II the values of the kinetic energy per particle at the critical temperature T_{c1} for several values of N used in the simulation.

The results of Table II agree qualitatively with the behavior observed in Fig. 6—the critical temperature decreases with the number of particles. The position of the discontinuity is reproduced reasonably well, and the agreement improves with increasing N. For $N = 160$ the discontinuity appears at $E_{\rm kin}/N = 0.72 \cdot 10^{-4}$ which is very close to the theory prediction of $0.79 \cdot 10^{-4}$.

C. The caloric curve

The simulation computed the average values of the total gas energy U/N and kinetic energy $E_{\rm kin}/N = \frac{1}{2}T$ per particle. We compare next the simulation result for the caloric curve with the theoretical prediction in (74).

Above the critical temperature the last term in the energy formula (74) vanishes, and we get, with the normalization of the simulation

$$\frac{U_{\rm sim}}{N} = \frac{1}{2}T + \frac{1}{24N} = \frac{E_{kin}}{N} + \frac{1}{24N}\,. \tag{78}$$

The kinetic energy per particle expressed as function of total energy per particle is a straight line with intercept $-\frac{1}{24N}$. For $N = 160$ this intercept is $-2.604 \cdot 10^{-4}$, which is very close to

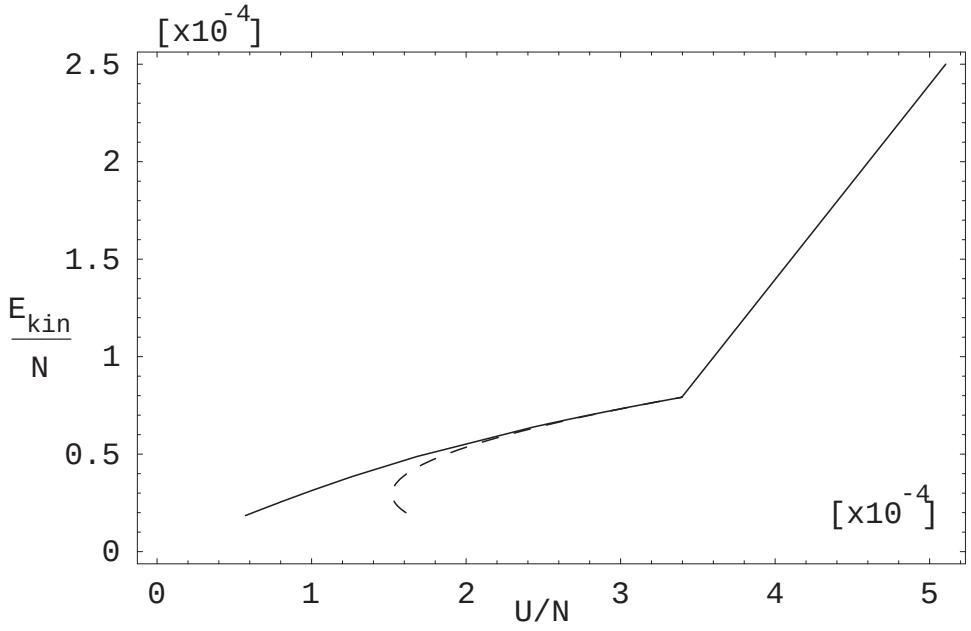

FIG. 12. Plot of the caloric curve $(U_{\rm sim}/N, E_{kin}/N)$ for $N = 160$. Dashed curve: approximative result using the approximation $K_1(\alpha) = \pi\alpha y_0^2$.

the intercept of the straight line observed in Fig. 7. Figure 13 presents a comparative plot of the theoretical and simulation data graphed together.

For temperatures below the critical temperature $T < T_{c1}$ the last term in the energy formula (74) starts contributing. In this region we have

$$\begin{aligned} \frac{U_{\rm sim}}{N} &= -\frac{1}{2}NT^2\int_0^1 dx[y'(x)]^2 + \frac{1}{2}T + \frac{1}{24N} \\ &= -2N\left(\frac{T}{2}\right)^2 K_1(\alpha) + \frac{1}{2}T + \frac{1}{24N} \end{aligned} \tag{79}$$

An analytical approximation for the integral $K_1(\alpha) = \int_0^1 dx[y'(x)]^2$ which is valid very close to the critical point is given in equation (47)

$$\begin{aligned} K_1(\alpha) \simeq \pi\alpha y_0^2 &= 24\pi\alpha\left(\sqrt{\frac{T_{c1}}{T}} - 1\right) \\ &= 24\pi\frac{1}{\sqrt{NT}}\left(\sqrt{\frac{1}{8\pi^2 N}\cdot\frac{2}{T}} - 1\right) \end{aligned} \tag{80}$$

The dashed curve in Figure 12 represents the result for the caloric curve following from this approximation. The solid curve shows the exact caloric curve obtained using the exact (numerical) result for $K_1(\alpha)$ in Table III. This table contains a tabulation of the integral

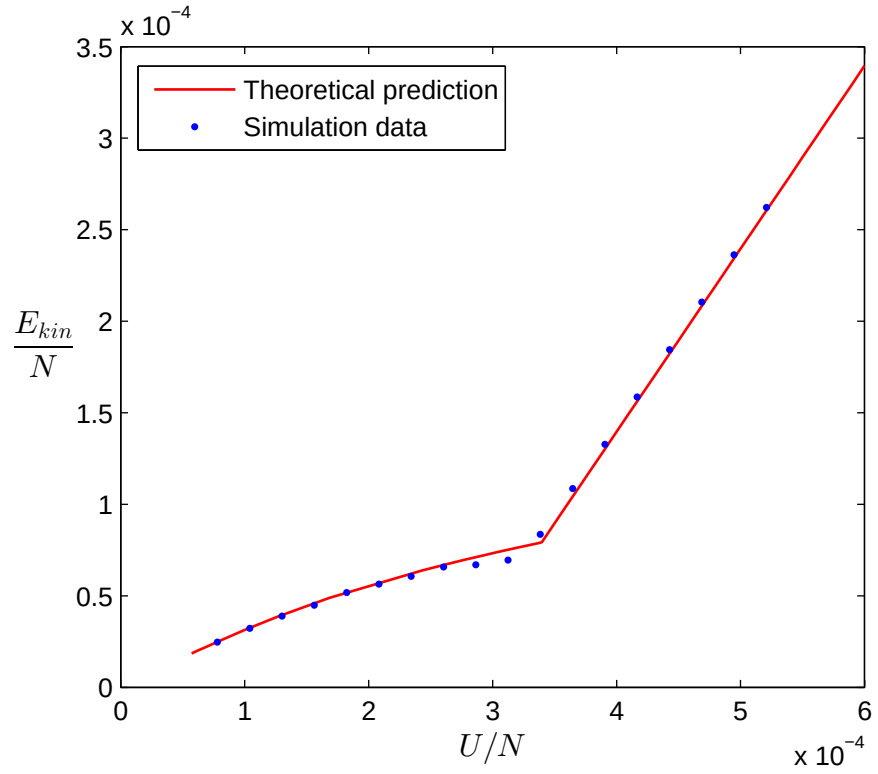

FIG. 13. Caloric curve: Theoretical prediction vs. simulation results for $N = 160$.

$K_1(\alpha)$ for values of α from 2π to 13. Each of these points corresponds to a value of the temperature, according to

$$\alpha^2 = (2\pi)^2 \frac{T_{c1}}{T} \tag{81}$$

From this we get the kinetic energy per particle

$$\frac{E_{kin}}{N} = \frac{1}{2}T = \frac{(2\pi)^2 T_{c1}}{\alpha^2} \tag{82}$$

The corresponding result for the total energy per particle is obtained from (79). Thus for each value of α in Table III we get a point with coordinates $(U_{\rm sim}/N, E_{\rm kin}/N)$. The set of all these points forms the caloric curve for temperatures below the critical temperatures shown in Figure 12.

D. Equation of state

The comparison of the simulation results for the pressure with the theoretical calculation is more difficult. It is known [41] that for systems with long-range interactions one has to

distinguish between the thermodynamical pressure (computed as $-(\partial F/\partial L)_{N,T}$) and the kinetic pressure (computed as in the numerical simulation). Additional complications have to be taken into account when using periodic boundary conditions [42].

In order to illustrate these issues, consider the case of a one-dimensional system of particles interacting by a constant attractive potential $V(x,y) = -cL$, proportional to the volume of the system L and $c > 0$. (Such a constant term is present in the interaction potential (4), where it appears because of imposing periodic boundary conditions.) The free energy is

$$F = -cNL - k_B T_V N \log L + F_{\rm kin} \tag{83}$$

which yields the thermodynamical pressure

$$p = k_B T_V \frac{N}{L} + cN \tag{84}$$

This is the ideal gas law, supplemented by the addition of a positive term. On the other hand it is clear that the kinetic pressure will not be changed by the constant potential $V(x,y) = -cL$ which corresponds to zero forces. This simple argument illustrates the difficulties encountered with the interpretation of the thermodynamical pressure in systems with long-range interactions. For these reasons we show only the results for the kinetic pressure obtained from the numerical simulation, see Figure 10.

VII. CONCLUSIONS

We studied in this paper the thermodynamical properties of a one-dimensional gas of N particles interacting via one-dimensional gravitational potentials, subject to periodic boundary conditions. This results in a modification of the two-body interaction potential which takes into account the contributions of an infinite number of mirror images (Ewald sum). The method of derivation is an application of Kiessling's approach to an infinite gravitational system where the potential is regularized by an exponential damping factor that is finally taken to the limit where the damping factor vanishes [36]. This model was proposed in Ref. [14] and was also used in Ref. [15] to describe a plasma consisting of charged particles in a uniform charge background. In this formulation each particle carries with it a uniformly distributed negative mass (or charge) background that arises from its infinite replicas. This should not be not confused with an external background potential that is introduced in an

ad-hoc approach. The system possesses complete translational invariance without imposing any additional constraints.

In carrying out our computations of the thermodynamic properties we considered the Vlasov limit, which corresponds to taking the particle number very large, at fixed volume (length) and total mass. In this limit the total energy and entropy have usual extensive properties, and we derived the exact solutions for the thermodynamical properties in the canonical ensemble.

In common with a gravitational system with an externally imposed background potential, the spatially periodic system considered here also undergoes a phase transition at a critical temperature T_{c1} [19]. Above the critical temperature the gas density is uniform, while below this temperature becomes non-uniform and has a stable unimodal density profile that is not fixed in position. Thus there is a continuum of solutions which differ only by a translation. Both the translationally invariant system considered here and the rigid system with externally imposed background potential exhibit an infinite sequence of critical points at which the system develops additional, unstable states. We show that only the inhomogeneous density state with unimodal density distribution appearing at T_{c1} is stable. This is in contrast with the free boundary self-gravitating system that has been studied extensively (for reviews see Refs.[38, 43]). For that system it was shown analytically by Rybicki that no phase transition occurs at any energy [4] in the one-dimensional gravitational system without hard core interaction. Note that in higher dimension it is necessary to screen the singularity of the gravitational force to obtain a phase transition[44–46].

Here we showed that the equilibrium density obeys a variant of the Lane-Emden equation which determines the gas density up to a translation. Both approximative and numerically-computed exact solutions for the thermodynamical properties were obtained and used to evaluate the internal energy and heat capacity as a function of temperature. A discontinuity in the slope of the caloric curve and corresponding discontinuity in the heat capacity, manifestations of a second order phase transition, were obtained.

In addition to the theoretical derivation of the thermodynamical properties, we carried out dynamical N-body simulations of the model which confirmed the analytically predicted features of the phase transition at the critical temperature T_{c1}. The temperature dependencies of the numerically-computed averages of the per-particle energy and pressure as well as the largest Lyapunov exponent display sudden changes in their slopes at $T \sim T_{c1}$. The

simulations utilized efficient event-driven algorithms that employed exact expressions for the time evolution of the system's phase-space and tangent-space vectors.

The long-range nature of the interaction potential of the model considered introduces known difficulties in the theoretical calculation of the equation of state in the inhomogeneous density state below the critical point. We plan on returning to this issue in future work. Nonetheless the simulation tools employed here allowed for the numerical estimations of the thermodynamic quantities and their corresponding behavior with changing temperature. Moreover, the μ-space distributions obtained in simulation confirm the existence of inhomogeneity in density below the critical temperature as predicted by our analytic treatment of the system.

Finally, it is worth highlighting that the discontinuity in the slope of the temperature dependence of the largest Lyapunov exponent displayed by our simulations near the critical temperature reaffirms the previously reported findings that suggested the applicability of the Lyapunov exponents as a possible indicator of phase transitions.

Appendix A: Appendix: Proof of the equation (7)

We give in this Appendix further details of the calculation of the sum over mirror images. This is done by writing the sum in (6) as

$$\sum_{k=-\infty}^{\infty} |x-y+kL| e^{-\kappa|x-y+kL|} \tag{A1}$$

$$= |x-y| e^{-\kappa|x-y|} + \sum_{n=-\infty}^{-1} (y-(x+nL)) e^{-\kappa(y-nL-x)} + \sum_{n=1}^{\infty} (x+nL-y) e^{-\kappa(x+nL-y)}$$

$$= |x-y| e^{-\kappa|x-y|} + \sum_{n=1}^{\infty} (y-(x-nL)) e^{-\kappa(y+nL-x)} + \sum_{n=1}^{\infty} (x+nL-y) e^{-\kappa(x+nL-y)}$$

$$= |x-y| e^{-\kappa|x-y|} + \sum_{n=1}^{\infty} nL e^{-\kappa nL} (e^{-\kappa(y-x)} + e^{\kappa(y-x)})$$

$$+ (y-x) \sum_{n=1}^{\infty} e^{-\kappa nL} (e^{-\kappa(y-x)} - e^{\kappa(y-x)}) \,. \tag{A2}$$

The sums over n can be evaluated in closed form

$$\sum_{n=1}^{\infty} e^{-\kappa nL} = \frac{1}{e^{\kappa L}-1} \tag{A3}$$

$$\sum_{n=1}^{\infty} nL e^{-\kappa nL} = L \frac{e^{\kappa L}}{(e^{\kappa L}-1)^2} \,. \tag{A4}$$

Substituting into the sums above gives equation (7).

Appendix B: Derivation of the free energy

We prove here the result (45) for the configurational contribution to the free energy per particle $f_Q[\rho]$. The starting point is the expression

$$f_Q = \frac{1}{2} T \int_0^1 dx \rho(x) \log \rho(x) - \frac{1}{2}\lambda - \frac{1}{2} T - T \log L \tag{B1}$$

which is obtained by eliminating the double integral in (23) using the Euler-Lagrange equation (24). Multiplying (24) with $\frac{1}{2}\rho(x)$ and integrating over x we get

$$\frac{1}{2} g^2 \int_0^1 dx dy \rho(x)\rho(y)(|x-y| - (x-y)^2 - \frac{1}{6}) = -\frac{1}{2} T \int_0^1 dx \rho(x) \log \rho(x) - \frac{1}{2}\lambda - \frac{1}{2} T \tag{B2}$$

Substituting this into (23) gives (B1).

We will evaluate the integral in the first term and the Lagrange multiplier, and will show that they are given by

$$J := \int_0^1 dx\rho(x)\log\rho(x) = \frac{3}{2\alpha^2}\int_0^1 dx[y'(x)]^2 + (1 - e^{y(0)} + y(0)) \tag{B3}$$

$$\lambda = -\frac{g^2}{\alpha^4}\int_0^1 dx[y'(x)]^2 + T(e^{y(0)} - y(0) - 2)\,. \tag{B4}$$

1. The calculation of the integral (B3). This is done by writing it as

$$J = \int_0^1 dx\rho(x)\log\rho(x) = \int_0^1 dx(1 - \frac{1}{\alpha^2}y''(x))y(x) = I_1 - \frac{1}{\alpha^2}I_2 \tag{B5}$$

where we used the Lane-Emden equation $y''(x) = \alpha^2(1-\rho(x))$ and evaluating the resulting integrals as follows.

There are two integrals appearing here.

$$I_1 := \int_0^1 dxy(x) = \frac{1}{2\alpha^2}\int_0^1 dx[y'(x)]^2 + 1 - e^{y(0)} + y(0) \tag{B6}$$

This follows from the relation (energy conservation for the equivalent dynamical problem)

$$\alpha^2(e^{y(0)} - y(0)) = \frac{1}{2}[y'(x)]^2 + \alpha^2(e^{y(x)} - y(x)) \tag{B7}$$

and integration over $x : (0,1)$ using the normalization condition $\int_0^1 dxe^{y(x)} = 1$.

The second integral is

$$I_2 := \int_0^1 dxy''(x)y(x) = y'(1)y(1) - y'(0)y(0) - \int_0^1 dx[y'(x)]^2 = -\int_0^1 dx[y'(x)]^2 \tag{B8}$$

where we used the boundary conditions $y(0) = y(1), y'(0) = y'(1)$.

2. Next we compute the Lagrange multiplier λ. This is expressed by taking $x = 0$ in the Euler-Lagrange equation (24) which gives

$$\lambda = -g^2\int_0^1 dx\rho(x)(x - x^2 - \frac{1}{6}) - T(\log\rho(0) + 1) \tag{B9}$$

The integral appearing here is evaluated by integration by parts. This is

$$\begin{aligned} I_3 &:= \int_0^1 dxe^{y(x)}(x - x^2 - \frac{1}{6}) = \int_0^1 dx(1 - \frac{1}{\alpha^2}y''(x))(x - x^2 - \frac{1}{6}) \qquad \text{(B10)}\\ &= -\frac{1}{\alpha^2}\int_0^1 dxy''(x)(x - x^2 - \frac{1}{6}) = -\frac{1}{\alpha^2}y'(x)(x - x^2 - \frac{1}{6})|_0^1 + \frac{1}{\alpha^2}\int_0^1 dxy'(x)(1 - 2x)\\ &= \frac{1}{\alpha^2}y(x)(1 - 2x)|_0^1 + \frac{1}{\alpha^2}2\int_0^1 dxy(x)\\ &= -\frac{2}{\alpha^2}y(0) + \frac{2}{\alpha^2}I_1 \end{aligned}$$

where the integral I_1 is given in (B6).

We get finally the result for the Lagrange multiplier

$$\lambda = -g^2 I_3 - T(y(0) + 1) \tag{B11}$$

where the integral I_3 is given in (B10). Combining all terms gives the result (B4).

ACKNOWLEDGMENTS

The authors benefited from insightful discussions with Dragos Anghel, Carlos Schat, Igor Prokhorenkov, Michael Kiessling, and Marc Miller.

TABLE III. Numerical solutions of the equation (36) for $\alpha \geq 2\pi$. Only the solution with $y_0 < 0$ is given; all other solutions can be obtained from this by a translation. We give also the values of the integral $K_k(\alpha)$ defined in (46). The column $\delta_k(\alpha) = 1 - e^{y_0} + y_0 + 1/\alpha^2 K_k$ gives the function appearing in the free energy difference with the $k = 0$ mode, see equation (62).

α	$y_1(0)$	$K_1(y_0)$	$\delta_1(\alpha)$	$y_2(0)$	$K_2(y_0)$	$\delta_2(\alpha)$
2π	0	0	0	-	-	-
6.3	-0.2646	1.27286	-0.00004	-	-	-
6.4	-0.7495	9.01418	-0.00203	-	-	-
6.5	-1.06682	17.0712	-0.00687	-	-	-
6.6	-1.335	25.4278	-0.01442	-	-	-
6.7	-1.5800	34.1811	-0.02453	-	-	-
6.8	-1.8084	43.2443	-0.03710	-	-	-
6.9	-2.0267	52.6788	-0.05200	-	-	-
7.0	-2.2377	62.4879	-0.06914	-	-	-
8.0	-4.2155	184.617	-0.34562	-	-	-
9.0	-6.2459	362.172	-0.77658	-	-	-
10.0	-8.4725	613.968	-1.33303	-	-	-
11.0	-10.9388	960.43	-2.00138	-	-	-
12.0	-13.6589	1423.37	-2.77439	-	-	-
4π	-15.3135	1745.99	-3.25689	0	0	0
12.6	-15.4145	1766.68	-3.28651	-0.2646	5.09144	-0.00004
12.7	-15.7162	1829.17	-3.37532	-0.5508	20.4223	-0.00067
12.8	-16.0205	1893.24	-3.46508	-0.7495	36.0567	-0.00203
12.9	-16.3272	1958.87	-3.55585	-0.917	52.0220	-0.00410
13.0	-16.6366	2026.14	-3.64761	-1.0668	68.2824	-0.00687

[1] S. Chandrasekhar, "An introduction to the theory of stellar structure," (1942).

[2] P.-H. Chavanis, Astronomy & Astrophysics **381**, 709 (2002).

[3] A. M. Salzberg, Journal of Mathematical Physics **6**, 158 (1965).

[4] G. B. Rybicki, Astrophysics and Space Science **14**, 56 (1971).

[5] A. Isihara, Physica **64**, 497 (1973).

[6] E. Presutti, *Scaling limits in statistical mechanics and microstructures in continuum mechanics* (Springer Science & Business Media, 2008).

[7] D. Pirjol and C. Schat, Journal of Mathematical Physics **56**, 013303 (2015).

[8] H. De Vega and N. Sanchez, Nuclear Physics B **625**, 409 (2002).

[9] J. Monaghan, Australian Journal of Physics **31**, 95 (1978).

[10] Y. Fukui and T. Morita, Australian Journal of Physics **32**, 289 (1979).

[11] M. E. Fisher and J. Lebowitz, Communications in Mathematical Physics **19**, 251 (1970).

[12] M. Antoni and S. Ruffo, Physical Review E **52**, 2361 (1995).

[13] T. Tatekawa, F. Bouchet, T. Dauxois, and S. Ruffo, Physical Review E **71**, 056111 (2005).

[14] B. N. Miller and J.-L. Rouet, Physical Review E **82**, 066203 (2010).

[15] P. Kumar and B. N. Miller, Phys. Rev. E **90**, 062918 (2014).

[16] E. Aurell and D. Fanelli, arXiv preprint cond-mat/0106444 (2001).

[17] D. Fanelli and E. Aurell, Astronomy & Astrophysics **395**, 399 (2002).

[18] E. Aurell, D. Fanelli, and P. Muratore-Ginanneschi, Physica D: Nonlinear Phenomena **148**, 272 (2001).

[19] P. Valageas, Astronomy & Astrophysics **450**, 445 (2006).

[20] P. Valageas, Physical Review E **74**, 016606 (2006).

[21] P. Kumar and B. N. Miller, Phys. Rev. E **93**, 040202 (2016).

[22] P. Kumar and B. N. Miller, arXiv preprint arXiv:1605.05780 (2016).

[23] G. Benettin, C. Froeschle, and J. P. Scheidecker, Phys. Rev. A **19**, 2454 (1979).

[24] N. Krylov, A. Migdal, Y. G. Sinai, and Y. L. Zeeman, Works on the Foundations of Statistical Physics by Nikolai Sergeevich Krylov translsated by AB Migdal, Ya. G. Sinai and Yu. L. Zeeman. Princeton Series in Physics. Published by Princeton University Press, Princeton, New Jersey 1979. (1979).

[25] I. PESIN, in *Akademiia Nauk SSSR, Doklady*, Vol. 226 (1976) pp. 774–777.

[26] Y. B. Pesin, Russian Mathematical Surveys **32**, 55 (1977).

[27] E. Ott, *Chaos in Dynamical Systems* (Cambridge University Press, 2002) pp. 137–145.

[28] J. Sprott, *Chaos and Time-series Analysis* (Oxford University Press, 2003) pp. 116–117.

[29] P. Butera and G. Caravati, Phys. Rev. A **36**, 962 (1987).

[30] L. Caiani, L. Casetti, C. Clementi, and M. Pettini, Phys. Rev. Lett. **79**, 4361 (1997).

[31] L. Casetti, M. Pettini, and E. G. D. Cohen, Physics Reports **337**, 237 (2000).

[32] C. Dellago and H. A. Posch, Physica A: Statistical Mechanics and its Applications **230**, 364 (1996).

[33] J. Barre and T. Dauxois, Europhysics Letters **55**, 164 (2001).

[34] A. Bonasera, V. Latora, and A. Rapisarda, Phys. Rev. Lett. **75**, 3434 (1995).

[35] V. Latora, A. Rapisarda, and S. Ruffo, Physica D: Nonlinear Phenomena **131**, 38 (1999).

[36] M. K.-H. Kiessling, Adv. Appl. Math. **31**, 132 (2003).

[37] J. Messer and H. Spohn, Journal of Statistical Physics **29**, 561 (1982).

[38] F. Bavaud, Reviews of Modern Physics **63**, 129 (1991).

[39] J. Landy *et al.*, European Journal of Physics **28**, 1051 (2007).

[40] D. McQuarrie, *Statistical Mechanics* (University Science Books, 2000) pp. 254–289.

[41] P. Choquard, P. Favre, and C. Gruber, Journal of Statistical Physics **23**, 405 (1980).

[42] M. J. Louwerse and E. J. Baerends, Chemical physics letters **421**, 138 (2006).

[43] Y. Levin, R. Pakter, F. B. Rizzato, T. N. Teles, and F. P. Benetti, Physics Reports **535**, 1 (2014).

[44] B. N. Miller and P. Youngkins, Phys. Rev. Lett. **81**, 4794 (1998).

[45] V. P. Youngkins and B. N. Miller, Physical Review E **62**, 4583 (2000).

[46] B. N. Miller, P. Klinko, and P. Youngkins, Chaos, Solitons & Fractals **13**, 603 (2002).